IOP PUBLISHING JOURNAL OF PHYSICS: CONDENSED MATTER

J. Phys.: Condens. Matter **24** (2012) 233203 (18pp) doi:10.1088/0953-8984/24/23/233203

TOPICAL REVIEW

Two-dimensional phonon transport in graphene

Denis L Nika[1] **and Alexander A Balandin**

Department of Electrical Engineering and Materials Science and Engineering Program, Bourns College of Engineering, University of California, Riverside, CA 92521, USA

E-mail: balandin@ee.ucr.edu

Received 1 February 2012, in final form 10 April 2012
Published 4 May 2012
Online at stacks.iop.org/JPhysCM/24/233203

Abstract

Properties of phonons—quanta of the crystal lattice vibrations—in graphene have recently attracted significant attention from the physics and engineering communities. Acoustic phonons are the main heat carriers in graphene near room temperature, while optical phonons are used for counting the number of atomic planes in Raman experiments with few-layer graphene. It was shown both theoretically and experimentally that transport properties of phonons, i.e. energy dispersion and scattering rates, are substantially different in a quasi-two-dimensional system such as graphene compared to the basal planes in graphite or three-dimensional bulk crystals. The unique nature of two-dimensional phonon transport translates into unusual heat conduction in graphene and related materials. In this review, we outline different theoretical approaches developed for phonon transport in graphene, discuss contributions of the in-plane and cross-plane phonon modes, and provide comparison with available experimental thermal conductivity data. Particular attention is given to analysis of recent results for the phonon thermal conductivity of single-layer graphene and few-layer graphene, and the effects of the strain, defects, and isotopes on phonon transport in these systems.

(Some figures may appear in colour only in the online journal)

Contents

[1] On leave from: Department of Theoretical Physics, Moldova State University, Republic of Moldova.

1. Introduction

Heat removal has become a crucial issue for continuing progress in the electronics industry owing to increased levels of dissipated power density and speed of electronic circuits [1]. Self-heating is a major problem in optoelectronics

and photonics [2]. These facts stimulated recent interest in thermal properties of materials. Acoustic phonons—fast moving quanta of the crystal lattice vibrations—are the main heat carriers in a variety of material systems. The phonon and thermal properties of nanostructures are substantially different from those of bulk crystals [3–15]. Semiconductor thin films or nanowires do not conduct heat as well as bulk crystals due to increased phonon–boundary scattering [4, 5] as well as changes in the phonon dispersion and density of states (DOS) [3–10]. However, theoretical studies suggested that phonon transport in strictly two-dimensional (2D) and one-dimensional (1D) systems can reveal exotic behavior, leading to infinitely large *intrinsic* thermal conductivity [11, 12]. These theoretical results have led to discussions of the validity of Fourier's law in low-dimensional systems [16, 17] and further stimulated interest in the acoustic phonon transport in 2D systems.

In this review, we focus on the specifics of the acoustic phonon transport in graphene. After a brief summary of the basics of thermal physics in nanostructures and experimental data for graphene's thermal conductivity, we discuss, in more detail, various theoretical approaches to calculation of the phonon thermal conductivity in graphene. Special attention is given to the analysis of the most recent theoretical and computational results on the relative contributions of different phonon polarization branches to the thermal conductivity of graphene. Readers interested in the experimental thermal conductivity values of graphene and related materials in the general context of carbon allotropes are referred to a different review [18].

2. Basics of phonon transport and thermal conductivity

The main experimental technique for investigation of the acoustic phonon transport in a given material system is the measurement of its lattice thermal conductivity [19, 20]. In this section, we define the main characteristics of heat conduction. The thermal conductivity is introduced through Fourier's law [21, 22]:

$$\vec{\phi} = -K\nabla T, \tag{1}$$

where $\vec{\phi}$ is the heat flux, ∇T is the temperature gradient and $K = (K_{\alpha\beta})$ is the thermal conductivity tensor. In the isotropic medium, thermal conductivity does not depend on the direction of the heat flow and K is treated as a constant. The latter is valid for small temperature variations only. In a wide temperature range, thermal conductivity is a function of temperature, i.e. $K \equiv K(T)$. In general, in solid materials heat is carried by phonons and electrons so that $K = K_\mathrm{p} + K_\mathrm{e}$, where K_p and K_e are the phonon and electron contributions, respectively. In metals or degenerately doped semiconductors, K_e is dominant due to the large density of free carriers. The value of K_e can be determined from the measurement of the electrical conductivity σ via the Wiedemann–Franz law [23]:

$$\frac{K_\mathrm{e}}{\sigma T} = \frac{\pi^2 k_\mathrm{B}^2}{3e^2}, \tag{2}$$

where k_B is the Boltzmann's constant and e is the charge of an electron. Phonons are usually the main heat carriers in carbon materials. Even in graphite, which has metal-like properties [24], the heat conduction is dominated by acoustic phonons [25]. This fact is explained by the strong covalent sp^2 bonding, resulting in high in-plane phonon group velocities and low crystal lattice anharmonicity for in-plane vibrations.

The phonon thermal conductivity can be written as

$$K_\mathrm{p} = \Sigma_j \int C_j(\omega)\upsilon_{x,j}(\omega)\upsilon_{x,j}(\omega)\tau_j(\omega)\,\mathrm{d}\omega, \tag{3}$$

where summation is performed over the phonon polarization branches j, which include two transverse acoustic branches and one longitudinal acoustic branch, $\upsilon_{x,j}$ is the projection of the phonon group velocity $\vec{\upsilon}_j = \mathrm{d}\omega_j/\mathrm{d}\vec{q}$ on the X axis for the jth branch, which, in many solids, can be approximated by the sound velocity, τ_j is the phonon relaxation time, $C_j = \hbar\omega_j \partial N_0(\hbar\omega_j/k_\mathrm{B}T)/\partial T$ is the contribution to heat capacity from the jth branch, and $N_0(\frac{\hbar\omega_j}{k_\mathrm{B}T}) = [\exp(\frac{\hbar\omega_j}{k_\mathrm{B}T}) - 1]^{-1}$ is the Bose–Einstein phonon equilibrium distribution function. The phonon mean free path (MFP) Λ is related to the relaxation time through the expression $\Lambda = \tau\upsilon$. In the relaxation-time approximation (RTA), various scattering mechanisms, which limit the MFP, are usually considered as additive, i.e. $\tau_j^{-1} = \sum_i \tau_{i,j}^{-1}$, where i denotes scattering mechanisms. In typical solids, acoustic phonons, which carry the bulk of the heat, are scattered by other phonons, lattice defects, impurities, conduction electrons, and interfaces [26–29].

In ideal crystals, i.e. crystals without lattice defects or rough boundaries, Λ is limited by the phonon–phonon scattering due to the crystal lattice anharmonicity. In this case, thermal conductivity is referred to as intrinsic. The anharmonic phonon interactions, which lead to the finite thermal conductivity in three dimensions, can be described by the umklapp processes [26]. The umklapp scattering rates depend on the Grüneisen parameter γ, which determines the degree of the lattice anharmonicity [26, 27]. Thermal conductivity is extrinsic when it is mostly limited by the extrinsic effects such as phonon–rough boundary or phonon–defect scattering.

In nanostructures, the phonon energy spectra are quantized due to the spatial confinement of the acoustic phonons. The quantization of the phonon energy spectra usually leads to decreasing phonon group velocity. The modification of the phonon energies, group velocities and density of states, together with phonon scattering from boundaries, affect the thermal conductivity of nanostructures. In most cases, the spatial confinement of acoustic phonons results in a reduction of the phonon thermal conductivity [30, 31]. However, it was predicted that the thermal conductivity of nanostructures embedded within the acoustically hard barrier layers can be increased via spatial confinement of acoustic phonons [6, 7, 10, 32].

The phonon–boundary scattering can be evaluated as [29]

$$\frac{1}{\tau_{\mathrm{B},j}} = \frac{\upsilon_{x,j}}{D}\frac{1-p}{1+p}, \tag{4}$$

where D is the nanostructure or grain size and p is the specularity parameter, defined as a probability of specular scattering at the boundary. The momentum-conserving specular scattering ($p = 1$) does not add to thermal resistance. Only diffuse phonon scattering from rough interfaces ($p \to 0$), which changes the phonon momentum, limits the phonon MFP. One can find p from the surface roughness or use it as a fitting parameter to experimental data. The commonly used expression for the phonon specularity is given by [29, 33, 34]

$$p(\lambda) = \exp\left(-\frac{16\pi^2\eta^2}{\lambda^2}\right), \quad (5)$$

where η is the root mean square deviation of the height of the surface from the reference plane and λ is the wavelength of the incident phonon.

In the case when the phonon–boundary scattering is dominant, thermal conductivity scales with the nanostructure or grain size D as $K_p \sim C_p \upsilon \Lambda \sim C_p \upsilon^2 \tau_B \sim C_p \upsilon D$. In the very small structures with $D \ll \Lambda$, the thermal conductivity dependence on the physical size of the structure becomes more complicated due to the strong quantization of the phonon energy spectra [6, 30, 32]. The specific heat C_p depends on the phonon density of states, which leads to different $C_p(T)$ dependences in three-dimensional (3D), two-dimensional and one-dimensional systems, and is reflected in the $K(T)$ dependence at low T [26, 29]. In bulk at low T $K(T) \sim T^3$, while $K(T) \sim T^2$ in 2D systems.

Thermal conductivity K defines how well a given material conducts heat. Another characteristic—thermal diffusivity, α—defines how fast the material conducts heat. Thermal diffusivity is given by the expression

$$\alpha = \frac{K}{C_p \rho_m}, \quad (6)$$

where ρ_m is the mass density. Many experimental techniques measure thermal diffusivity rather than thermal conductivity.

3. Experimental data for thermal conductivity of graphene

We start by providing a brief summary of the experimental data available for the thermal conductivity of graphene. The first measurements of heat conduction in graphene [35–40] were carried out at UC Riverside in 2007 (see figure 1). The investigation of the phonon transport was made possible by the development of the optothermal Raman measurement technique. The experiments were performed with large-area suspended graphene layers exfoliated from high-quality Kish and highly ordered pyrolytic graphite. It was found that the thermal conductivity varies in a wide range and can exceed that of the bulk graphite, which is ~2000 W mK^{-1} at room temperature (RT). It was also determined that the electronic contribution to heat conduction in the ungated graphene near RT is much smaller than that of phonons, i.e. $K_e \ll K_p$. The phonon MFP in graphene was estimated to be of the order of 800 nm near RT [36].

Several independent studies, which followed, also utilized the Raman optothermal technique but modified it via addition of a power meter under the suspended portion of graphene. It was found that the thermal conductivity of suspended high-quality chemical vapor deposited (CVD) graphene exceeded ~2500 W mK^{-1} at 350 K, and it was as high as $K \approx 1400$ W mK^{-1} at 500 K [41]. The reported value was also larger than the thermal conductivity of bulk graphite at RT. Another Raman optothermal study with the suspended graphene found the thermal conductivity in the range from ~1500 to ~5000 W mK^{-1} [42]. Another group that repeated the Raman-based measurements found $K \approx 630$ W mK^{-1} for a suspended graphene membrane [43]. The differences in the actual temperature of graphene under laser heating, strain distribution in the suspended graphene of various sizes and geometries can explain the data variation.

Another experimental study reported the thermal conductivity of graphene to be ~1800 W mK^{-1} at 325 K and ~710 W mK^{-1} at 500 K [44]. These values are lower than that of bulk graphite. However, instead of measuring the light absorption in graphene under conditions of their experiment, the authors of [44] assumed that the optical absorption coefficient should be 2.3%. It is known that, due to many-body effects, the absorption in graphene is a function of wavelength λ, when $\lambda > 1$ eV [45–47]. The absorption of 2.3% is observed only in the near-infrared at ~1 eV. The absorption steadily increases with decreasing λ (increasing energy). The 514.5 nm and 488 nm Raman laser lines correspond to 2.41 eV and 2.54 eV, respectively. At 2.41 eV the absorption is about $1.5 \times 2.3\% \approx 3.45\%$ [45]. The value of 3.45% is in agreement with the one reported in another independent study [48]. Replacing the assumed 2.3% with 3.45% in the study reported in [44] gives ~2700 W mK^{-1} at 325 K and 1065 W mK^{-1} near 500 K. These values are higher than those for the bulk graphite and consistent with the data reported by other groups [41, 48], where the measurements were conducted by the same Raman optothermal technique but with the measured light absorption.

The data for suspended or partially suspended graphene is closer to the intrinsic thermal conductivity because suspension reduces thermal coupling to the substrate and scattering on the substrate defects and impurities. The thermal conductivity of fully supported graphene is smaller. The measurements for exfoliated graphene on SiO_2/Si revealed in-plane $K \approx$ 600 W mK^{-1} near RT [49]. Solving the Boltzmann transport equation (BTE) and comparing with their experiments, the authors determined that the thermal conductivity of free graphene should be ~3000 W mK^{-1} near RT.

Despite the noted data scatter in the reported experimental values of the thermal conductivity of graphene, one can conclude that it is very large compared to that for bulk silicon ($K = 145$ W mK^{-1} at RT) or bulk copper ($K = 400$ W mK^{-1} at RT)—important materials for electronic applications. The differences in K of graphene can be attributed to variations in the graphene sample lateral sizes (length and width), thickness nonuniformity due to the mixing between single-layer and few-layer graphene, material quality (e.g. defect concentration and surface contaminations), grain size and orientation, as well as strain distributions. Often the reported thermal conductivity values of graphene corresponded to different

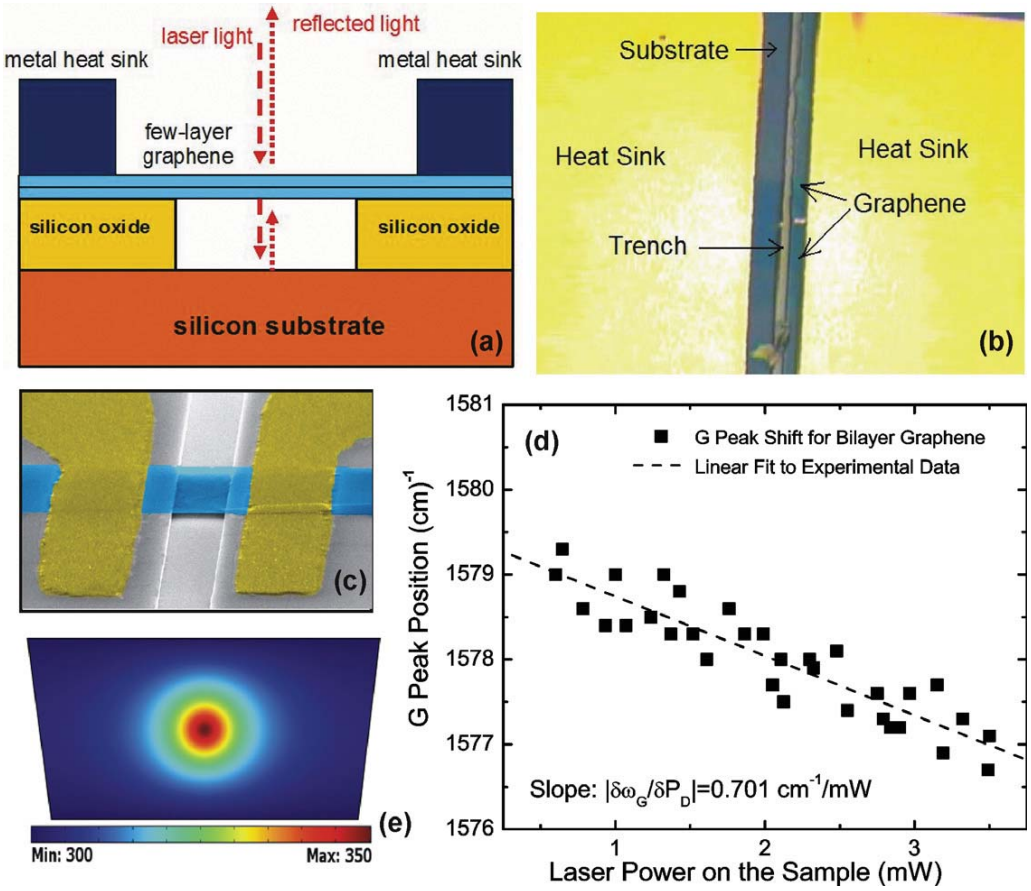

Figure 1. Illustration of optothermal micro-Raman measurement technique developed for investigation of phonon transport in graphene. (a) Schematic diagram of the thermal conductivity measurement showing suspended FLG flakes and excitation laser light. (b) Optical microscopy images of FLG attached to metal heat sinks. (c) Colored scanning electron microscopy image of the suspended graphene flake to clarify typical structure geometry. (d) Experimental data for Raman *G*-peak position as a function of laser power, which determines the local temperature rise in response to the dissipated power. (e) Finite-element simulation of temperature distribution in the flake with the given geometry used to extract the thermal conductivity. Reproduced with permission from [38]. Copyright 2010 Nature Publishing Group.

sample temperatures T, despite the fact that the measurements were conducted at ambient temperature. The strong heating of the samples was required due to the limited spectral resolution of the Raman spectrometers used for temperature measurements. Naturally, the thermal conductivity values determined at ambient temperature but for the samples heated to $T \sim 350$ and 600 K over a substantial portion of their area would be different and cannot be directly compared. One should also note that the data scatter for thermal conductivity of carbon nanotubes (CNTs) is much larger than that for graphene. For a more detailed analysis of the experimental uncertainties the readers are referred to a comprehensive review [18].

4. Phonon transport in suspended few-layer graphene

The phonon thermal conductivity undergoes an interesting evolution when the system dimensionality changes from 2D to 3D. This evolution can be studied with the help of suspended few-layer graphene (FLG) with increasing thickness H–number of atomic planes n. It was reported in [38] that thermal conductivity of suspended uncapped FLG decreases with increasing n approaching the bulk graphite limit (see figure 2). This trend was explained by considering the intrinsic quasi-2D crystal properties described by the phonon umklapp scattering [38]. As n in FLG increases, the phonon dispersion changes and more phase space states become available for phonon scattering, leading to thermal conductivity decrease. The phonon scattering from the top and bottom boundaries in suspended FLG is limited if constant n is maintained over the layer length. The small thickness of FLG ($n < 4$) also means that phonons do not have a transverse cross-plane component in their group velocity, leading to an even weaker boundary scattering term for the phonons. In thicker FLG films the boundary scattering can increase due to the nonzero cross-plane phonon velocity component. It is also harder to maintain constant thickness through the whole area of the FLG flake. These factors can lead to a thermal conductivity below the graphite limit. The graphite value is recovered for thicker films.

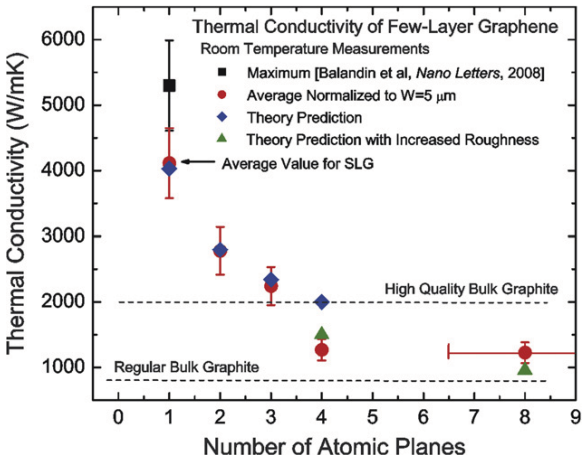

Figure 2. Measured thermal conductivity as a function of the number of atomic planes in suspended FLG. The dashed straight lines indicate the range of bulk graphite thermal conductivities. The blue diamonds were obtained from the first-principles theory of thermal conduction in FLG based on the actual phonon dispersion and accounting for all allowed three-phonon umklapp scattering channels. The green triangles are Callaway–Klemens model calculations, which include extrinsic effects characteristic of thicker films. Reproduced with permission from [38]. Copyright 2010 Nature Publishing Group.

The experimentally observed evolution of the thermal conductivity in FLG with n varying from 1 to $n \sim 4$ [38] is in agreement with the theory for the crystal lattices described by the Fermi–Pasta–Ulam Hamiltonians [50]. The molecular dynamics (MD) calculations for graphene nanoribbons with the number of planes n from one to eight [51] also gave a thickness dependence of the thermal conductivity in agreement with the UC Riverside experiments [38]. The strong reduction of the thermal conductivity as n changes from one to two is in line with the earlier theoretical predictions [52]. In another reported study, the Boltzmann transport equation was solved under the assumptions that in-plane interactions are described by the Tersoff potential while the Lennard-Jones potential models interactions between atoms belonging to different layers [53, 54]. The obtained results suggested a strong thermal conductivity decrease as n changed from one to two and slower decrease for $n > 2$.

The thermal conductivity dependence on the FLG is entirely different for the encased FLG where thermal transport is limited by the acoustic phonon scattering from the top and bottom boundaries and disorder. The latter is common when FLG is embedded between two layers of dielectrics. An experimental study [55] found $K \approx 160$ W mK^{-1} for encased single-layer graphene (SLG) at $T = 310$ K. It increases to $\sim$1000 W mK^{-1} for graphite films with the thickness of 8 nm. It was also found that the suppression of thermal conductivity in encased graphene, as compared to bulk graphite, was stronger at low temperatures, where K was proportional to T^{β} with $1.5 < \beta < 2$ [55]. Thermal conduction in encased FLG was limited by the rough boundary scattering and disorder penetration through graphene.

5. Phonon spectra in graphene, few-layer graphene and graphene nanoribbons

Intriguing thermal and electrical properties of graphene, FLG [18, 35–38, 55–58] and graphene nanoribbons (GNRs) [59–61] stimulate investigations of phonon energy spectra in these materials and structures [62–76]. The phonon energy spectrum is important for determining the sound velocity, phonon density of states, phonon–phonon or electron–phonon scattering rates, and lattice heat capacity, as well as the phonon thermal conductivity. The optical phonon properties manifest themselves in Raman measurements. The number of graphene layers and their quality and stacking order can be clearly distinguished using Raman spectroscopy [38, 77–80]. For these reasons, significant efforts have been made to accurately determine the phonon energy dispersion in graphite [62–65], graphene [38, 53, 66–71, 76] and GNRs [72–75, 81], and to reveal specific features of their phonon modes.

The phonon dispersion in graphite along the Γ–M–K–Γ directions (see figure 3(a), where the graphene Brillouin zone is shown) measured by x-ray inelastic scattering was reported in [62, 63]. A number of research groups calculated the phonon energy dispersion in graphite, graphene and GNRs using various theoretical approaches, including the continuum model [74, 75], Perdew–Burke–Ernzerhof generalized gradient approximation (GGA) [62, 64, 65], first-order local density function approximation (LDA) [64, 66, 70], fourth- and fifth-nearest neighbor force constant (4NNFC and 5NNFC) approaches [63, 65, 71] and Born–von Karman or valence force field (VFF) model of the lattice dynamics [38, 67, 68, 76], and utilized the Tersoff and Brenner potentials [69] or Tersoff and Lennard-Jones potentials [53, 54]. GGA and LDA models are *ab initio* models, while all other models are based on different sets of the fitting parameters, which are determined from comparison with the experimental phonon dispersion [62, 63, 82].

The number of parameters in the theoretical models depends on the model specifics and the number of atomic neighbors considered. The number of parameters varies from five [65] to 23 [71]. For example, our VFF model for graphene used only six parameters [76]. In this model, all interatomic forces are resolved into bond-stretching and bond-bending forces [76, 83–85]. This model takes into account stretching and bending interactions with two in-plane and two out-of-plane atomic neighbors as well as doubled stretching–stretching interactions with the nearest in-plane neighbors [76]. The honeycomb crystal lattice of graphene utilized in this model is presented in figure 3(b). The rhombic unit cell of graphene, shown as a dashed region, contains two atoms and is defined by two basis vectors, $\vec{a}_1 = a(3, \sqrt{3})/2$ and $\vec{a}_2 = a(3, -\sqrt{3})/2$, where $a = 0.142$ nm is the distance between two nearest carbon atoms. The six phonon polarization branches $s = 1, \ldots, 6$ in SLG are shown in figure 4. These branches are (i) out-of-plane acoustic (ZA) and out-of-plane optical (ZO) phonons with the displacement vector along the Z axis; (ii) transverse acoustic (TA) and transverse optical (TO) phonons, which corresponds

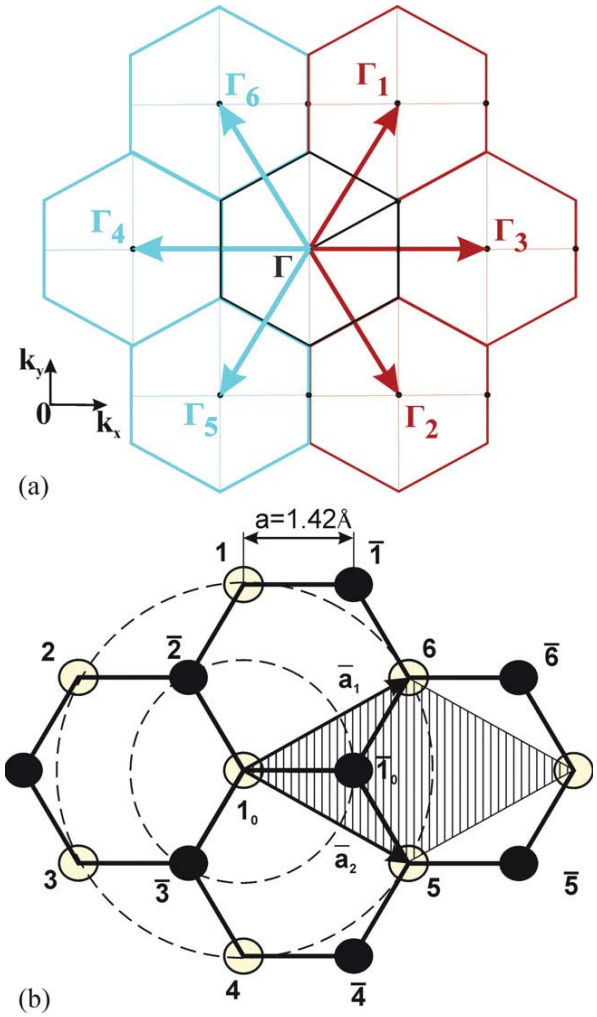

Figure 3. (a) Reciprocal lattice of graphene. (b) Graphene crystal lattice. The rhombic unit cell is shown as a shaded region. Reproduced with permission from [76]. Copyright 2009 American Physical Society.

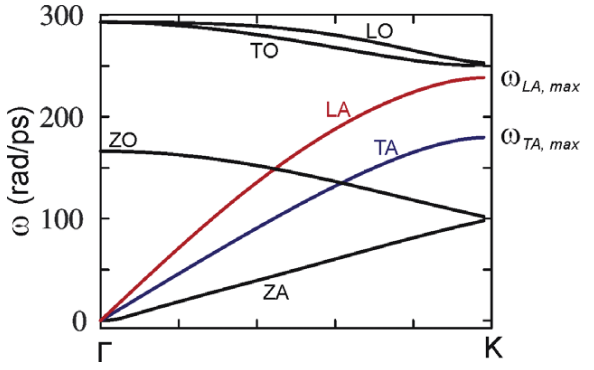

Figure 4. Phonon frequencies ω_s in graphene calculated using the valence force field model [37].

to the transverse vibrations within the graphene plane; (iii) longitudinal acoustic (LA) and longitudinal optical (LO) phonons, which corresponds to the longitudinal vibrations within the graphene plane.

Although various theoretical models are in qualitative agreement with each other, they predict substantially different phonon frequencies at the Γ, M or K points of the Brillouin zone. Moreover, some of the models give the same frequencies for the LO–LA phonons [65, 66, 69] and ZO–TA phonons [63, 64, 67, 76] at the M point, while the rest of the models predict different frequencies for these phonons at the M point [62, 68, 70]. The comparison between phonon frequencies at the high-symmetry points of the Brillouin zone is presented in tables 1 and 2. The discrepancy in the calculated phonon dispersion can easily translate into differences in the predicted thermal conductivity values. Specifically, the relative contributions of the LA, TA, and ZA phonons to heat transport can vary in a wide range depending on the specifics of the phonon dispersion used.

The unit cell of the n-layer graphene contains $2n$ atoms, therefore $6n$ quantized phonon branches appear in n-layer graphene. In figures 5(a) and (b) we show the phonon dispersions in bilayer graphene. Weak van der Waals interaction between monolayers leads to the coupling of long-wavelength phonons only and quantization of the low-energy part of the spectrum with $q < 0.1q_{\max}$ for LA, TA, LO, TO and ZO phonons and with $q < 0.4q_{\max}$ for ZA phonons (see figure 5(b)). The modification of the phonon energy spectrum in n-layer graphene as compared with that in single-layer graphene results in a substantial change of the three-phonon scattering rates and a reduction of the intrinsic thermal conductivity in n-layer graphene [38, 53, 54].

6. Specifics of the acoustic phonon transport in two-dimensional crystals

We now address in more detail some specifics of the acoustic phonon transport in 2D systems. Investigation of the heat conduction in graphene [35, 36] and CNTs [86] raised the issue of ambiguity in the definition of the intrinsic thermal conductivity for 2D and 1D crystal lattices. It was theoretically shown that the intrinsic thermal conductivity limited by the crystal anharmonicity has a finite value in 3D bulk crystals [12, 50]. However, many theoretical models predict that the intrinsic thermal conductivity reveals a logarithmic divergence in strictly 2D systems, $K \sim \ln(N)$, and a power-law divergence in 1D systems, $K \sim N^{\alpha}$, with the number of atoms N $(0 < \alpha < 1)$ [12, 16, 50, 86–90]. The logarithmic divergence can be removed by introduction of the *extrinsic* scattering mechanisms such as scattering from defects or coupling to the substrate [50]. Alternatively, one can define the *intrinsic* thermal conductivity of a 2D crystal for a given size of the crystal.

Graphene is not an ideal 2D crystal, considered in most of the theoretical works, since graphene atoms vibrate in three directions. Nevertheless, the intrinsic graphene thermal conductivity strongly depends on the graphene sheet size due to weak scattering of the low-energy phonons by other

Table 1. Energies of ZO and LO phonons at the Γ point in graphite and graphene.

Sample	Γ_{ZO} (cm^{-1})	Γ_{LO} (cm^{-1})	Comments	References
Graphite	—	1583[a]	Experiment: x-ray scattering	[a][62]
Graphite	—	1581[b]	Experiment: x-ray scattering	[b][63]
Graphite	899[c]	1593[c]	Theory: LDA	[c][64]
Graphite	∼820[a], 879[c], 881[c]	1559[c], 1561[c], 1581–1582[a]	Theory: GGA	[d][82]
Graphite	868[b]	1577[b]	Theory: 5NNFC	[e][65]
Graphite	∼920[d]	∼1610[d]	Theory: six-parameter force constant model	[f][66]
Graphene	879[c], 881[c], 884[e]	1554[c], 1559[c], 1569[e]	Theory: GGA	[g][70]
Graphene	890[g], 896[g], ∼900[f]	1586[f], 1595[g], 1597[g]	Theory: LDA	
Graphene	893	1581	Theory: Born–von Karman	[67]
Graphene	889[h], 883.5[i]	1588[h], 1555[i]	Theory: VFF model	[h][68], [i][76]
Graphene	∼1300	∼1685	Theory: optimized Tersoff	[69]
	∼1165	∼1765	Theory: optimized Brenner	

Table 2. Phonon energies at K and M points in graphite and graphene.

Sample	K_{ZA} (cm^{-1})	K_{TA} (cm^{-1})	K_{LA} (cm^{-1})	Comments	References
Graphite	—	—	1194[a]	Experiment: x-ray scattering; $\omega_{LO}(M) > \omega_{LA}(M)$;	[a][62]
Graphite	542[b]	1007[b]	1218[b]	Experiment: x-ray scattering; $\omega_{LO}(M) > \omega_{LA}(M)$; $\omega_{ZO}(M) \approx \omega_{TA}(M)$	[b][63]
Graphite	—	—	—	Experiment: high-resolution electron-energy-loss spectroscopy; $\omega_{LO}(M) > \omega_{LA}(M)$; $\omega_{ZO}(M) < \omega_{TA}(M)$	[82]
Graphite	540[c]	1009[c]	1239[c]	Theory: LDA; $\omega_{LO}(M) > \omega_{LA}(M)$ $\omega_{ZO}(M) \approx \omega_{TA}(M)$	[c][64] [d][65]
Graphite	534[c], 540[c]	∼960[a], 998[c], 999[c]	1220[a], 1216[c], 1218[c]	Theory: GGA; [a,c]$\omega_{LO}(M) > \omega_{LA}(M)$; [c]$\omega_{ZO}(M) \approx \omega_{TA}(M)$	
Graphite	542[b]	1007[b]	1218[b]	Theory: 5NNFC; $\omega_{LO}(M) > \omega_{LA}(M)$; $\omega_{ZO}(M) \approx \omega_{TA}(M)$	
Graphene	535[c], 539[d]	997[c], 1004[d]	1213[c], 1221[d]	Theory: GGA; [c]$\omega_{LO}(M) > \omega_{LA}(M)$; [d]$\omega_{LO}(M) \approx \omega_{LA}(M)$; [c,d]$\omega_{ZO}(M) \approx \omega_{TA}(M)$	
Graphene	∼520[e,f]	∼990[f], ∼1000[e]	∼1250[f], ∼1220[e]	Theory: LDA; [e]$\omega_{LO}(M) \approx \omega_{LA}(M)$; [e]$\omega_{ZO}(M)\omega_{ZA}(M) \ll \omega_{TA}(M)$[f]$\omega_{LO}(M) > \omega_{LA}(M)$; [f]$\omega_{ZO}(M) > \omega_{ZA}(M)$;	[e][66] [f][70]
Graphene	495	1028	1199	Theory: Born–von Karman model; $\omega_{LO}(M) > \omega_{LA}(M)$; $\omega_{ZO}(M) \approx \omega_{TA}(M)$	[67]
Graphene	544[g], 532[h]	1110[g], 957[h]	1177[g], 1267[h]	Theory: VFF model; [g,h]$\omega_{LO}(M) > \omega_{LA}(M)$; [g]$\omega_{ZO}(M) < \omega_{TA}(M)$; [h]$\omega_{ZO}(M) \approx \omega_{TA}(M)$	[g][68] [h][76]
Graphene	∼635	∼1170	∼1170	Theory: optimized Tersoff potential; $\omega_{LO}(M) \approx \omega_{LA}(M)$; $\omega_{ZO}(M) > \omega_{TA}(M)$	[69]
	∼585	∼1010	∼1240	Theory: optimized Brenner potential; $\omega_{LO}(M) > \omega_{LA}(M)$; $\omega_{ZO}(M) > \omega_{TA}(M)$	

phonons in the system. Therefore, the phonon–boundary scattering is an important mechanism for phonon relaxation in graphene. Different studies [91, 92] also suggested that an accurate accounting for the higher-order anharmonic processes, i.e. above three-phonon umklapp scattering, and inclusion of the normal phonon processes in consideration, allow one to limit the low-energy phonon MFP. The normal phonon processes do not contribute directly to thermal

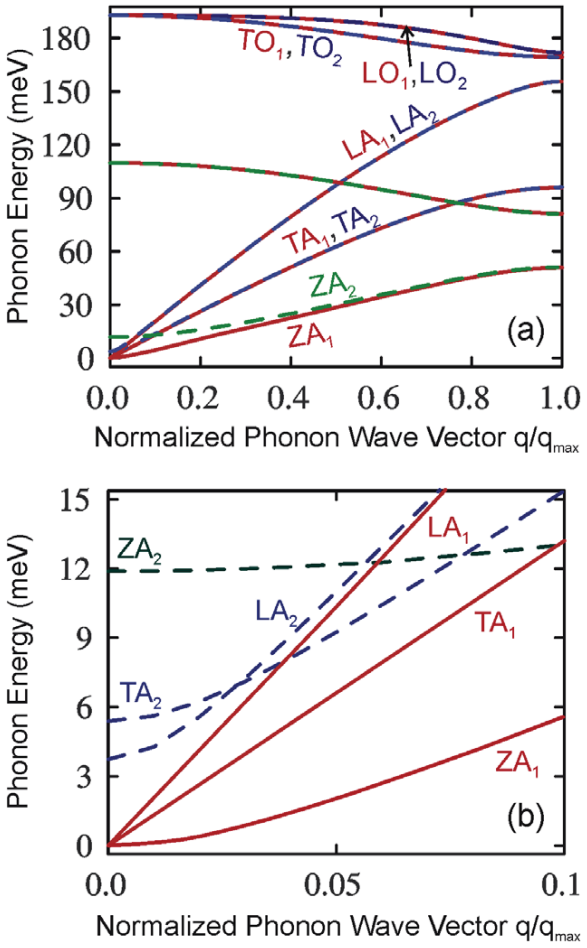

Figure 5. Phonon energy spectra in bilayer graphene calculated using the valence force field model shown for (a) the Γ–M direction and (b) near the Brillouin zone center. Reproduced with permission from [38]. Copyright 2010 Nature Publishing Group.

resistance but affect the phonon mode distribution [53, 93]. However, even these studies found that the graphene sample has to be very large (>10 μm) to obtain the size-independent thermal conductivity.

The specific phonon transport in a quasi-2D system such as graphene can be illustrated with an expression derived by Klemens specifically for graphene [25, 94]. In the framework of the BTE approach and the RTA, the intrinsic umklapp-limited thermal conductivity of graphene can be written as [25, 94]

$$K = \frac{\rho_{\mathrm{m}}}{2\pi\gamma^2}\frac{\bar{\upsilon}^4}{f_{\mathrm{m}}T}\ln\left(\frac{f_{\mathrm{m}}}{f_{\mathrm{B}}}\right). \tag{7}$$

Here, f_{m} is the upper limit of the phonon frequencies defined by the phonon dispersion, $\bar{\upsilon}$ is the average phonon group velocity and $f_{\mathrm{B}} = \left(M\bar{\upsilon}^3 f_{\mathrm{m}}/4\pi\gamma^2 k_{\mathrm{B}}TL\right)^{1/2}$ is the size-dependent low-bound cut-off frequency for acoustic phonons, introduced by limiting the phonon MFP with the graphene layer size L.

In [95] we improved equation (7) by taking into account the actual maximum phonon frequencies and Grüneisen parameters $\gamma_s(s = \mathrm{TA}, \mathrm{LA})$ determined separately for LA and TA phonon branches. The Grüneisen parameters were computed by averaging the phonon mode-dependent $\gamma_s(\vec{q})$ for all relevant phonons (here $\vec{q}$ is the wavevector):

$$K = \frac{1}{4\pi k_{\mathrm{B}}T^2 h}\sum_{s=\mathrm{TA,LA}}\int_{q_{\min}}^{q_{\max}}\left\{\left[\hbar\omega_s(q)\frac{\mathrm{d}\omega_s(q)}{\mathrm{d}q}\right]^2 \times \tau^K_{\mathrm{U},s}(q)\frac{\exp[\hbar\omega_s(q)/k_{\mathrm{B}}T]}{[\exp[\hbar\omega_s(q)/k_{\mathrm{B}}T]-1]^2}q\right\}\mathrm{d}q. \tag{8}$$

Here $\hbar\omega_s(q)$ is the phonon energy, $h = 0.335$ nm is the graphene layer thickness and $\tau^K_{\mathrm{U},s}(q)$ is the three-phonon mode-dependent umklapp relaxation time, which was derived using an expression from [25, 26] but introducing separate lifetimes for LA and TA phonons:

$$\tau^K_{\mathrm{U},s} = \frac{1}{\gamma_s^2}\frac{M\bar{\upsilon}_s^2}{k_{\mathrm{B}}T}\frac{\omega_{s,\max}}{\omega^2}, \tag{9}$$

where $s = \mathrm{TA}, \mathrm{LA}$, $\bar{\upsilon}_s$ is the average phonon velocity for a given branch, $\omega_{s,\max} = \omega(q_{\max})$ is the maximum cut-off frequency for a given branch and M is the mass of a graphene unit cell. In [25, 94, 95] the contribution of ZA phonons to thermal transport has been neglected because of their low group velocity and large Grüneisen parameter γ_{ZA} [64, 95]. equation (9) can be used to calculate thermal conductivity with the actual dependence of the phonon frequency $\omega_s(q)$ and the phonon velocity $\mathrm{d}\omega_s(q)/\mathrm{d}q$ on the phonon wavenumber. To simplify the model, one can use the linear dispersion $\omega_s(q) = \bar{\upsilon}_s q$ and re-write it as

$$K_{\mathrm{U}} = \frac{\hbar^2}{4\pi k_{\mathrm{B}}T^2 h} \times \sum_{s=\mathrm{TA,LA}}\int_{\omega_{\min}}^{\omega_{\max}}\left\{\omega^3\tau^K_{\mathrm{U},s}(\omega)\frac{\exp[\hbar\omega/kT]}{[\exp[\hbar\omega/kT]-1]^2}\right\}\mathrm{d}\omega. \tag{10}$$

Substituting equation (9) to (10) and performing integration one obtains

$$K_{\mathrm{U}} = \frac{M}{4\pi Th}\sum_{s=\mathrm{TA,LA}}\frac{\omega_{s,\max}\bar{\upsilon}_s^2}{\gamma_s^2}F(\omega_{s,\min}, \omega_{s,\max}), \tag{11}$$

where

$$F(\omega_{s,\min}, \omega_{s,\max}) = \int_{\hbar\omega_{s,\min}/k_{\mathrm{B}}T}^{\hbar\omega_{s,\max}/k_{\mathrm{B}}T}\xi\frac{\exp(\xi)}{[\exp(\xi)-1]^2}\,\mathrm{d}\xi = \left[\ln\{\exp(\xi)-1\} + \frac{\xi}{1-\exp(\xi)} - \xi\right]\Bigg|_{\hbar\omega_{s,\min}/k_{\mathrm{B}}T}^{\hbar\omega_{s,\max}/k_{\mathrm{B}}T}. \tag{12}$$

In the above equation, $\xi = \hbar\omega/k_{\mathrm{B}}T$, and the upper cut-off frequencies $\omega_{s,\max}$ are defined from the actual phonon dispersion in graphene (see figure 4): $\omega_{\mathrm{LA,max}} = 2\pi f_{\mathrm{LA,max}}(\Gamma\mathrm{K}) = 241$ rad ps^{-1}, $\omega_{\mathrm{TA,max}} = 2\pi f_{\mathrm{TA,max}}(\Gamma\mathrm{K}) = 180$ rad ps^{-1}.

The integrand in equation (12) can be further simplified near RT when $\hbar\omega_{s,\max} > k_B T$, and it can be expressed as

$$F(\omega_{s,\min}) \approx -\ln\{|\exp(\hbar\omega_{s,\min}/k_B T) - 1|\} + \frac{\hbar\omega_{s,\min}}{k_B T}\frac{\exp(\hbar\omega_{s,\min}/k_B T)}{\exp(\hbar\omega_{s,\min}/k_B T) - 1}. \quad (13)$$

There is a clear difference between the heat transport in basal planes of bulk graphite and in single-layer graphene [25, 94]. In the former, the heat transport is approximately two dimensional only up to some lower-bound cut-off frequency $\omega_{\min}$. Below $\omega_{\min}$ there appears to be strong coupling with the cross-plane phonon modes and heat starts to propagate in all directions, which reduces to negligible values the contributions of these low-energy modes to heat transport along basal planes. In bulk graphite, there is a physically reasonable reference point for the onset of the cross-plane coupling, which is the ZO′ phonon branch near ∼4 THz observed in the spectrum of bulk graphite [25, 96]. The presence of the ZO′ branch and corresponding $\omega_{\min} = \omega_{ZO'}$ $(q = 0)$ allows one to avoid the logarithmic divergence in the umklapp-limited thermal conductivity integral (see equations (10)–(13)) and calculate it without considering other scattering mechanisms.

The physics of heat conduction is principally different in graphene, where the phonon transport is 2D all the way to zero phonon frequency $\omega(q = 0) = 0$. There is no onset of the cross-plane heat transport at the long-wavelength limit in the system, which consists of only one atomic plane. This is no ZO′ branch in the phonon dispersion of graphene (see figure 4). Therefore, the lower-bound cut-off frequencies $\omega_{s,\min}$ for each s are determined from the condition that the phonon MFP cannot exceed the physical size L of the flake, i.e.

$$\omega_{s,\min} = \frac{\bar{\upsilon}_s}{\gamma_s}\sqrt{\frac{M\bar{\upsilon}_s}{k_B T}\frac{\omega_{s,\max}}{L}}. \quad (14)$$

We would like to emphasize here that using size-independent graphite $\omega_{\min}$ for SLG or FLG (as has been proposed in [97]) is without scientific merit and leads to an erroneous calculation of thermal conductivity, as described in detail in [98]. Equations (12)–(14) constitute a simple analytical model for the calculation of the thermal conductivity of the graphene layer, which retains such important features of graphene phonon spectra as different $\bar{\upsilon}_s$ and γ_s for LA and TA branches. The model also reflects the two-dimensional nature of heat transport in graphene all the way down to zero phonon frequency.

In figure 6, we present the dependence of thermal conductivity of graphene on the dimension of the flake L. The data are presented for the averaged values of the Grüneisen parameters $\gamma_{LA} = 1.8$ and $\gamma_{TA} = 0.75$ obtained from *ab initio* calculations, as well as for several other close sets of $\gamma_{LA,TA}$ to illustrate the sensitivity of the result to the Grüneisen parameters. For small graphene flakes, the K dependence on L is fairly strong. It weakens for flakes with $L \geq 10$ μm. The calculated values are in good agreement with available experimental data for suspended exfoliated [35, 36] and CVD graphene [41, 42]. The horizontal dashed line indicates the experimental thermal conductivity for bulk graphite, which is exceeded by graphene's thermal conductivity at smaller L. Thermal conductivity, presented in figure 6, is an *intrinsic* quantity limited by the three-phonon umklapp scattering only. But it is determined for a specific graphene flake size since L defines the lower-bound (long-wavelength) cut-off frequency in umklapp scattering through equation (14). In experiments, thermal conductivity is also limited by defect scattering. When the size of the flake becomes very large with many polycrystalline grains, the scattering on their boundaries will also lead to phonon relaxation. The latter can be included in our model through adjustment of L. The extrinsic phonon scattering mechanisms or high-order phonon–phonon scatterings prevent indefinite growth of thermal conductivity of graphene with L.

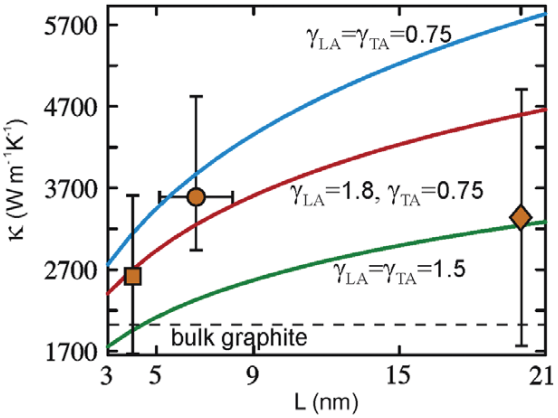

Figure 6. Calculated room-temperature thermal conductivity of graphene as a function of the lateral size for several values of the Grüneisen parameter. Experimental data points from [35, 36] (circle), [41] (square) and [42] (rhomb) are shown for comparison.

7. The *Q*-space diagram theory of phonon transport in graphene

The simple models described in the previous section are based on the Klemens-like expressions for the relaxation time (see equation (9)). Therefore, they do not take into account all peculiarities of the 2D three-phonon umklapp processes in SLG or FLG, which are important for the accurate description of thermal transport. There are two types of three-phonon umklapp scattering process [26]. The first type is the scattering when a phonon with the wavevector $\vec{q}(\omega)$ absorbs another phonon from the heat flux with the wavevector $\vec{q}'(\omega')$, i.e. the phonon leaves the state $\vec{q}$. For this type of scattering process the momentum and energy conservation laws are written as

$$\vec{q}(\omega) + \vec{q}'(\omega') = \vec{b}_i + \vec{q}''(\omega''), \qquad i = 1, 2, 3$$
$$\omega + \omega' = \omega'', \quad (15)$$

The processes of the second type are those when the phonons $\vec{q}(\omega)$ of the heat flux decay into two phonons with the wavevectors $\vec{q}'(\omega')$ and $\vec{q}''(\omega'')$, i.e. leave the state $\vec{q}(\omega)$,

or, alternatively, two phonons $\vec{q}'(\omega')$ and $\vec{q}''(\omega'')$ merge together, forming a phonon with the wavevector $\vec{q}(\omega)$, which corresponds to the phonon coming to the state $\vec{q}(\omega)$. The conservation laws for this type are given by

$$\begin{aligned} \vec{q}(\omega) + \vec{b}_i &= \vec{q}'(\omega') + \vec{q}''(\omega''), \qquad i = 4, 5, 6 \\ \omega &= \omega' + \omega''. \end{aligned} \tag{16}$$

In equations (15) and (16) $\vec{b}_i = \Gamma\bar{\Gamma}_i$, $i = 1, 2, \ldots, 6$ is one of the vectors of the reciprocal lattice (see figure 3(a)).

Calculations of the thermal conductivity in graphene taking into account all possible three-phonon umklapp processes allowed by equations (15) and (16) and actual phonon dispersions were carried out for the first time in [76]. For each phonon mode (q_i, s), all pairs of the phonon modes $(\vec{q}', s')$ and $(\vec{q}'', s'')$ were found such that the conditions of equations (15) and (16) are met. As a result, in $(\vec{q}')$ space the *phase diagrams* were constructed for all allowed three-phonon transitions [76]. Using the long-wave approximation (LWA) for a matrix element of the three-phonon interaction, the authors of [76] obtained for the umklapp scattering rates

$$\begin{aligned} \frac{1}{\tau_{\mathrm{U}}^{(\mathrm{I}),(\mathrm{II})}(s, \vec{q})} &= \frac{\hbar\gamma_s^2(\vec{q})}{3\pi\rho\upsilon_s^2(\vec{q})} \\ &\times \sum_{s's'';\vec{b}_i} \iint \omega_s(\vec{q})\omega'_{s'}(\vec{q}')\omega''_{s''}(\vec{q}'') \\ &\times \{N_0[\omega'_{s'}(\vec{q}')] \mp N_0[\omega''_{s''}(\vec{q}'')] + \tfrac{1}{2} \mp \tfrac{1}{2}\} \\ &\times \delta[\omega_s(\vec{q}) \pm \omega'_{s'}(\vec{q}') - \omega''_{s''}(\vec{q}'')]\, \mathrm{d}q'_l\, \mathrm{d}q'_\perp. \end{aligned} \tag{17}$$

Here q'_l and $q'_\perp$ are the components of the vector $\vec{q}'$ parallel or perpendicular to the lines defined by equations (15) and (16), respectively, $\gamma_s(\vec{q})$ is the mode-dependent Grüneisen parameter, which is determined for each phonon wavevector and polarization branch, and ρ is the surface mass density. In equation (17) the upper signs correspond to the processes of the first type while the lower signs correspond to those of the second type. The integrals for q_l and $q_\perp$ are taken along and perpendicular to the curve segments, respectively, where the conditions of equations (15) and (16) are met. Integrating along $q_\perp$ in equation (17) one can obtain the line integral

$$\begin{aligned} \frac{1}{\tau_{\mathrm{U}}^{(\mathrm{I}),(\mathrm{II})}(s, \vec{q})} &= \frac{\hbar\gamma_s^2(\vec{q})\omega_s(\vec{q})}{3\pi\rho\upsilon_s^2(\vec{q})} \sum_{s's'';\vec{b}} \int_l \frac{\pm(\omega''_{s''} - \omega_s)\omega''_{s''}}{\upsilon_{\perp,s'}(\omega'_{s'})} \\ &\times (N'_0 \mp N''_0 + \tfrac{1}{2} \mp \tfrac{1}{2})\, \mathrm{d}q'_l. \end{aligned} \tag{18}$$

The phonon scattering on the rough edges of graphene can be evaluated using equation (4). The total phonon relaxation rate is given by

$$\frac{1}{\tau_{\mathrm{tot}}(s, q)} = \frac{1}{\tau_{\mathrm{U}}(s, q)} + \frac{1}{\tau_{\mathrm{B}}(s, q)}. \tag{19}$$

The sensitivity of the room temperature thermal conductivity, calculated using equations (17)–(19), to the value of the specular parameter of phonon–boundary scattering is illustrated in figure 7. The data are presented for different sizes (widths) of the graphene flakes. The experimental data points for suspended exfoliated [35, 36] and CVD [41, 42] graphene are also shown for comparison. Table 3 provides representative experimental and theoretical data for the suspended and supported graphene.

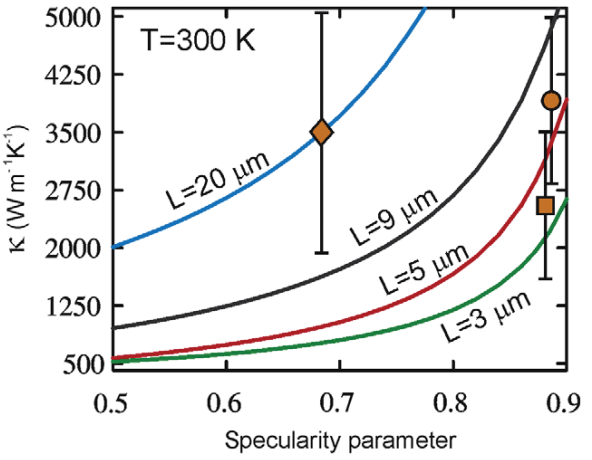

Figure 7. Calculated room-temperature thermal conductivity of suspended graphene as a function of the specularity parameter p for the phonon scattering from the flake edges. Note a strong dependence on the size of the graphene flakes. Experimental data points from [35, 36] (circle), [41] (square) and [42] (rhomb) are shown for comparison.

8. Thermal conductivity of graphene nanoribbons

Measurements of thermal properties of graphene stimulated a surge of interest in theoretical and experimental studies of heat conduction in graphene nanoribbons [59–61, 81, 99–110]. It is important to understand how lateral sizes affect the phonon transport properties from both fundamental science and practical application points of view. In the last few years a number of theoretical works investigated phonon transport and heat conduction in graphene nanoribbons with various lengths, widths, edge roughnesses and defect concentrations. The authors used MD simulations [59–61, 99–102], the nonequilibrium Green's function method [103–105] and BTE approaches [81, 106].

Keblinsky and co-workers [59] found from the MD study that the thermal conductivity of graphene is $K \approx$ 8000–10 000 W mK^{-1} at RT for the square graphene sheet. The K value was size independent for $L > 5$ nm [59]. For the ribbons with fixed $L = 10$ nm and width W varying from 1 to 10 nm, K increased from ∼1000 W mK^{-1} to 7000 W mK^{-1}. The thermal conductivity in GNRs with rough edges can be suppressed by orders of magnitude as compared to that in GNRs with perfect edges [59, 61]. The isotopic superlattice modulation of GNRs or defects of crystal lattices also significantly decreases the thermal conductivity [104, 105]. The uniaxial stretching applied in the longitudinal direction enhances the low-temperature thermal conductance for the 5 nm armchair or zigzag GNRs to 36% due to the stretching-induced convergence of phonon spectra to the low-frequency region [103].

Table 3. Thermal conductivity of graphene and graphene nanoribbons.

Sample	K (W mK^{-1})	Method	Comments	References
Graphene	∼2000–5000	Raman optothermal	Suspended; exfoliated	[35, 36]
FLG	1300–2800	Raman optothermal	Suspended; exfoliated; $n = 2$–4	[38]
Graphene	∼2500	Raman optothermal	Suspended; CVD	[41]
Graphene	∼1500–5000	Raman optothermal	Suspended; CVD	[42]
Graphene	600	Raman optothermal	Suspended; exfoliated; $T \sim 660$ K	[43]
Graphene	600	Electrical	Supported; exfoliated;	[49]
FLG nanoribbon	1100	Electrical self-heating	Supported; exfoliated; $n < 5$	[109]
FLG nanoribbon	80–150	Electrical self-heating	Supported	[110]
Graphene	∼2430	Theory: BTE, third-order IFCs	$K(graphene) \geq K(carbon\,nanotube)$	[93]
Graphene	1000–8000	Theory: BTE + RTA γ_{LA}, γ_{TA}	Strong size dependence	[95]
Graphene	2000–8000	Theory: BTE + RTA, $\gamma_s(q)$	Strong edge, width and Grüneisen parameter dependence	[76]
Graphene	∼4000	Theory: ballistic	Strong width dependence	[60]
Graphene	500–1100	Theory: molecular dynamic, optimized Tersoff	$T \sim 435$ K, calculation domain $4.4 \times 4.3 \times 1.6$ nm^3: periodic boundary condition	[111]
Graphene	∼2900	Theory: MD simulation	Strong dependence on the vacancy concentration	[112]
Graphene	1500–3500	Theory: BTE, third-order IFCs	Strong size dependence	[113]
FLG	1000–4000	Theory: BTE + RTA, $\gamma_s(q)$	$n = 8 - 1$, strong size dependence	[38]
FLG	1000–3500	Theory: BTE, third-order IFCs	$n = 5 - 1$, strong size dependence	[53]
FLG	2000–3300	Theory: BTE, third-order IFCs	$n = 4 - 1$	[54]
FLG	580–880	Theory: MD simulation	$n = 5 - 1$, strong dependence on the van der Waals bond strength	[114]
GNR	1000–7000	Theory: molecular dynamics, Tersoff	Strong ribbon width and edge dependence	[59]
GNR	∼5500	Theory: BTE + RTA	GNR with width of 5 μm; strong dependence on the edge roughness	[81]

Aksamija and Knezevic [81] calculated the dependence of the thermal conductivity of a GNR with the width 5 μm and RMS edge roughness $\Delta = 1$ nm on temperature (see figure 8). The thermal conductivity was calculated taking into account the three-phonon umklapp, mass-defect and rough edge scatterings [81]. The authors obtained RT thermal conductivity $K \sim 5500$ W mK^{-1} for the 5-μm-wide suspended graphene ribbon. The study of the nonlinear thermal transport in rectangular and triangular GNRs under large temperature biases was reported in [107]. The authors found that, in short (∼6 nm) rectangular GNRs, a negative differential thermal conductance exists in a certain range of the applied temperature difference. As the length of the rectangular GNR increases the effect weakens. A computational study reported in [108] predicted that the combined effects of the edge roughness and local defects play a dominant role in determining the thermal transport properties of zigzag GNRs. The experimental data on thermal transport in GNRs are very limited. In [109] the authors used an electrical self-heating method and extracted the thermal conductivity of sub-20 nm GNRs to be more than 1000 W mK^{-1} at 700–800 K. However, this study assumed that the thermal resistance of the graphene–substrate interface is the same as that of the carbon–substrate interface [109], which is likely to have led to a higher value of K. A similar experimental method but with more accurate account of the GNRs' thermal coupling to the substrate has been used in [110]. Liao *et al* [110] found substantially lower values of thermal conductivity of ∼80–150 W mK^{-1} at RT. The calculated and measured data for the thermal conductivity of graphene nanoribbons are also given in table 3. We would like to note that the BTE and MD models used for calculations of the thermal conductivity in graphene and GNRs depend on the interatomic potentials while MD simulations are also sensitive to the size of the simulation domains. The differences in the potentials and domain sizes are some of the reasons for the observed data scatter for the thermal conductivity in different works.

9. Analysis of recent theoretical results

In this section we review and analyze the most recent theoretical results pertinent to phonon transport in graphene. Ong and Pop [115] examined thermal transport in graphene supported on SiO_2 using MD simulations. The approach employed by the authors utilized the reactive empirical bond order (REBO) potential to model the atomic interaction between the C atoms, Munetoh potential to model the atomic

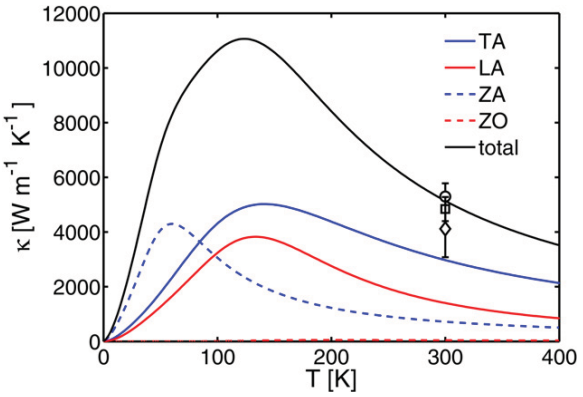

Figure 8. Thermal conductivity results for graphene ribbon of width $W = 5$ μm and RMS edge roughness $\Delta = 1$ nm, showing contributions from individual phonon branches TA, LA, ZA, and ZO and total. Experimental data points from [35, 36] are shown for comparison. Reproduced with permission from [81]. Copyright 2011 American Institute of Physics.

interactions between the Si and O atoms and Lennard-Jones potential to model the van der Waals type C–Si and C–O couplings. The authors suggested that thermal conductivity in supported graphene is smaller by an order of magnitude than that in suspended graphene due to damping of the out-of-plane ZA phonons. Surprisingly, Ong and Pop [115] found from their calculations that increasing the strength of the graphene–substrate interactions further can enhance the heat flow and effective thermal conductivity along the supported graphene. The authors attributed this result to the coupling of graphene ZA modes to the substrate Rayleigh waves, which linearizes the phonon dispersion, increases the group velocity of the hybridized modes and, thus, enhances the thermal flux. One should note here that Seol *et al* [49] concluded from their experiments and calculations that graphene's coupling to its substrate leads to additional phonon scattering with the corresponding reduction of the in-plane thermal conductivity of graphene. The comparison of the computational [115] and experimental [49] results calls for additional studies of thermal properties of graphene supported on different substrates.

Qiu and Ruan [111, 116] addressed the problem of relative contributions of ZA phonons to thermal transport in the framework of the equilibrium MD simulations. Their conclusion was that in suspended SLG out-of-plane ZA phonons are coupled with in-plane phonons due to the third-order and higher-order anharmonic interactions, which results in about 25%–30% contribution of ZA phonons to the thermal conductivity of graphene. In supported SLG the contribution of all acoustic and ZO phonon branches are reduced owing to the SLG–substrate interface scattering and breakdown of the symmetries for both in-plane and out-of-plane phonons. The contributions of ZA phonons to thermal conductivity are suppressed more strongly than the contributions of TA and LA phonons. Qiu and Ruan [111, 116] stated that the in-plane TA and LA phonons are the dominant heat carriers in supported SLG and make a major contribution in suspended SLG.

The strain effects on the thermal conductivity of graphene and GNRs were studied computationally in [117]. The authors used MD simulations and found that the thermal conductivity of graphene is very sensitive to the tensile strain. It was shown that when the strains are applied in both directions—parallel and perpendicular to the heat transfer path—the graphene sheets undergo complex reconstructions. As a result, some of the strained graphene structures can have higher thermal conductivity than that of SLG without strain [117]. The suggested strong strain dependence of the thermal conductivity of graphene can explain some of discrepancies in the reported experimental values of the thermal conductivity of suspended graphene. The suspended graphene flakes and membranes are expected to have different strain fields depending on the size and geometry of the suspected graphene sample.

The strong dependence of the thermal conductivity of graphene on the defect concentration was established in the computational studies reported in [112, 118]. Both studies used MD simulations. According to Hao *et al* [118], 2% of the vacancies or other defects can reduce the thermal conductivity of graphene by as much as a factor of five to ten. Zhang *et al* [112] determined from their MD simulations that the thermal conductivity of pristine graphene should be ∼2903 W mK^{-1} at RT. According to their calculations the thermal conductivity of graphene can be reduced by a factor of 1000 at the vacancy defect concentration of ∼9%. The numeric results of [112, 118] suggest another possible explanation of the experimental data scatter, which is different defect densities in the examined graphene samples. For example, if the measurements of the thermal conductivity of graphene by the thermal bridge technique give smaller values than those by the Raman optothermal technique, one should take into account that the thermal bridge technique requires a substantial number of fabrication steps, which result in residual defects.

An intriguing question in the theory of phonon transport in graphene is a relative contribution to heat conduction by LA, TA and ZA phonon polarization branches. The calculations of the thermal conductivity from BTE within RTA [25, 94, 95, 119] or by using the three-phonon matrix elements obtained from the LWA [76] show relatively small—down to negligible—contributions of ZA phonons. The latter is mainly attributed to the large (negative) Grüneisen parameter, which defines the strength of phonon scattering in anharmonic processes, and the small phonon group velocity. However, there is an alternative description of phonon transport in graphene. Lindsay, Broido, Mingo and co-workers [49, 53, 113] reported the first calculations of the thermal conductivity of graphene in the framework of the linearized BTE and three-phonon matrix elements based on the third-order interatomic force constants (IFCs). Their calculations suggested that heat conduction is dominated by the ZA phonons. The latter results from the mode-dependent third-order IFCs and a special selection rule in ideal graphene, which restricts the phase space for the phonon–phonon scattering, thus increasing the ZA phonon lifetime. The authors of [49, 53, 113] also emphasized the importance of the

three-phonon *normal* processes for an accurate description of the thermal conductivity of graphene and few-layer graphene. However, for comparison with experimental data, one should note that placing graphene on any substrate and the presence of nanoscale corrugations in graphene lattice would break the symmetry selection rule, thus allowing ZA phonons to scatter. It is also possible that ZA dispersion undergoes modification, e.g. linearization, due to the substrate coupling, as suggested by Ong and Pop [115].

More recently, Singh *et al* [54, 120] followed the theoretical approach of [53, 113] to determine the relative contribution of the polarization branches, and analyze the effect of different theoretical approximations used for graphene [120], including the classical phonon statistics, LWA and omission of the normal three-phonon processes. Thermal conductivities calculated under various assumptions were compared with that obtained from solving the linearized BTE [120] with the phonon scattering strengths computed using the anharmonic IFCs written as

$$\Phi_{\alpha\beta\gamma}(0k, l'k', l''k'') = \frac{\partial^3 V}{\partial u_\alpha(0k)\partial u_\beta(l'k')\partial u_\gamma(l''k'')}, \quad (20)$$

where $u_\alpha(lk)$ is the αth component of a displacement of the kth atom in the lth unit cell and $V = V(c_1, c_2, \ldots, c_N)$ is the empirical interatomic potential. The number of constants in a set $(c_1, c_2, \ldots, c_N)$ depends on the type of interatomic potential, while values of the constants are usually determined from comparison of the calculated cohesive energy, phonon energy or another measurable quantity with the experimental data.

To determine $\Phi_{\alpha\beta\gamma}(0k, l'k', l''k'')$, Singh *et al* [120] employed the optimized Tersoff interatomic potential with the set of parameters determined by Lindsay and Broido [69] from the fitting of the phonon frequencies and the zone-center group velocities. Nevertheless, the optimized Tersoff potential gives a rather poor agreement with the available experimental frequencies ω for ZO phonons near the Γ point (the difference is about 80 rad ps^{-1} at the Γ point), ZO, LO and TA phonons near the M point (the difference is about 40–50 rad ps^{-1} for both phonons at the M point) and ZA, TA and LO phonons near the K point (the difference is about 20 rad ps^{-1} for ZA, 40 rad ps^{-1} for TA and 100 rad ps^{-1} for LO phonons at the K point) (see figure 1 from [69]). Moreover, the phonon energies and group velocities of TA phonons, calculated using this potential, are overestimated over half of the Brillouin zone. The phonon energies were found as a solution of a set of equations of motion which depends on the *second-order* (harmonic) IFCs only (see equation (1) from [54]),

$$\Phi_{\alpha\beta}(0k, l'k') = \frac{\partial^2 V}{\partial u_\alpha(0k)\partial u_\beta(l'k')}. \quad (21)$$

Therefore, the calculation of the *third-order* IFCs $\Phi_{\alpha\beta\gamma}(0k, l'k', l''k'')$, which are important for the thermal transport and for determining the relative contribution of LA, TA, ZA phonons to the thermal conductivity, is not a well justified procedure and can lead to inaccurate conclusions about the importance of the phonon branches for heat conduction.

It is known that the elastic and vibration properties depend strongly on the type of the empirical potential as shown in many theoretical publications [121–124]. Broido *et al* [121] demonstrated that the Tersoff and environment-dependent interatomic potentials give vastly different thermal expansion and Grüneisen coefficients. Cowley [122] analyzed vibration properties of silicon using Stillinger–Weber and Tersoff potentials and concluded that none of these potentials provide a fully satisfactory description of the lattice vibrations. Sevincli *et al* [123] demonstrated that LA and TA modes in the hybrid boron nitride–graphene sheets are equally well described by the Tersoff potential and the fourth-nearest-neighbor force constants while the energies of ZA, ZO, TO and LO phonons are not. The influence of different interatomic potentials on the thermal conductivity is discussed in [124]. The higher-order phonon processes can also change the relative contributions of different phonons to the thermal conductivity. In their classical MD simulations, Qiu and Ruan [111, 116] predicted strong coupling of ZA phonons with LA and TA phonons due to the higher-order umklapp and normal processes with a corresponding increase of their scattering. In their calculation, ZA phonons accounted for 15% in the graphene on the substrate and ∼25%–30% in the suspended SLG [111, 116].

For all the reasons discussed above, we consider the question of the relative contributions of different phonon polarizations to the thermal conductivity of graphene to be still open. Experimentally, it is difficult to address this question. Measurements of the temperature dependence of the thermal conductivity cannot present evidence in favor of one or the other phonon contribution because the $K(T)$ dependence in graphite is known to be strongly influenced by the material quality [55, 125, 126]. One should note here that despite the differences in the theoretical models and assumptions the theoretical results obtained for the RT thermal conductivity of graphene are relatively close. The RT thermal conductivity of SLG found by Nika *et al* [38, 76] using RTA and LWA is $K \sim 4000$ W mK^{-1}, which is close to the results of Lindsay *et al* [53, 69, 113] found from BTE with the optimized potentials: $K = 3500$ W mK^{-1} (Tersoff) and $K = 3600$ W mK^{-1} (Brenner). Singh *et al* [54, 120], who used a model similar to that of [53, 69, 113], obtained $K \sim 3250$ W mK^{-1}.

10. Isotope effects on phonon transport in graphene

Naturally occurring carbon materials are made up of two stable isotopes of ^{12}C (∼99%) and ^{13}C (∼1%). The change in isotope composition modifies dynamic properties of crystal lattices and affects their thermal conductivity. The isotopically purified materials are characterized by enhanced thermal conductivity [127–131]. The knowledge of isotope effects on thermal properties is valuable for understanding phonon transport. The isotope composition affects directly the phonon relaxation rates in the phonon mass-difference scattering processes. The phonon scattering rate on point defects, $1/\tau_P$, is given as [25, 119] $1/\tau_P \propto V_0(\omega^\alpha/\upsilon_j^\beta)\Upsilon$, where V_0 is the volume per atom in the crystal lattice, Υ is the strength of the

phonon–point defect scattering, and $\alpha = 3\,(4)$ and $\beta = 2\,(3)$ for a 2D (3D) system, respectively. In the perturbation theory Υ can be written as [25, 119]

$$\Upsilon = \sum_i f_i[(1 - M_i/\bar{M})^2 + \varepsilon(\gamma(1 - R_i/\bar{R}))^2], \qquad (22)$$

where f_i is the fractional concentration of the substitutional foreign atoms, e.g. impurity, defect or isotope atoms, M_i is the mass of the ith substitutional atom, $\bar{M} = \sum_i f_i M_i$ is the average atomic mass, R_i is the Pauling ionic radius of the ith foreign atom, $\bar{R} = \sum_i f_i R_i$ is the average radius and ε is a phenomenological parameter. The mass of a foreign atom—impurity, vacancy, defect or isotope—is well known, while the local displacement $\Delta R = \bar{R} - R_i$ due to the atom radius or bond-length difference is usually not known well.

One can see from equation (22) that the phonon–isotope scattering is unique in the sense that, unlike impurity or defect scattering, it involves only the well defined mass-difference term, $\Delta M = \bar{M} - M_i$, without the ambiguous volume or bond-strength difference term, $\Delta R = \bar{R} - R_i$ or ε. As the system dimensionality changes from 3D to 2D, the phonon scattering on point defects undergoes additional modification owing to the different phonon DOSs. The change in the phonon DOS reveals itself via dependence of $1/\tau_P$ on ω and υ. Thus, the isotope effects in graphene are particularly important for understanding its thermal properties and, more generally, for development of theory of the phonon transport in low-dimensional systems.

The first experimental study of the isotope effects on the thermal properties of graphene was reported just recently [132]. The isotopically modified graphenes containing various percentages of ^{13}C were synthesized by the CVD technique [133, 134]. The regions of different isotopic composition were parts of the same graphene sheet to ensure uniformity in material parameters. The thermal conductivity of the isotopically pure ^{12}C (0.01% ^{13}C) graphene, determined by the optothermal Raman technique [18, 35, 36, 38, 41, 48], was higher than 4000 W mK^{-1} at the temperature $T \sim 320$ K, and more than a factor of two higher than the value of K in a graphene sheet composed of a 50%–50% mixture of ^{12}C and ^{13}C.

Figure 9 shows thermal conductivity in the isotopically modified graphene as a function of temperature. The evolution of thermal conductivity with the isotope content was attributed to the changes in the phonon–point defect scattering rate $1/\tau_P$ via the mass-difference term $\Delta M = \bar{M} - M_i$. The phonon υ and mass density do not undergo substantial modification with the isotope composition. The relative change in the phonon velocity $\upsilon_{^{12}C}/\upsilon_{\text{natural}}$ is related to the mass densities of the respective lattices $\upsilon_{^{12}C}/\upsilon_{\text{natural}} = (M_{\text{natural}}/M_{^{12}C})^{1/2}$. Removal of 1% ^{13}C in natural diamond causes the velocity to increase only by a tiny fraction, which cannot account for the observed strong change in the thermal conductivity.

The reported experimental data in [132] agree well with the authors' own MD simulations, corrected for the long-wavelength phonon contributions via the Klemens model [132] and other numeric data reported previously [76, 135, 136]. A recent study [137] reported

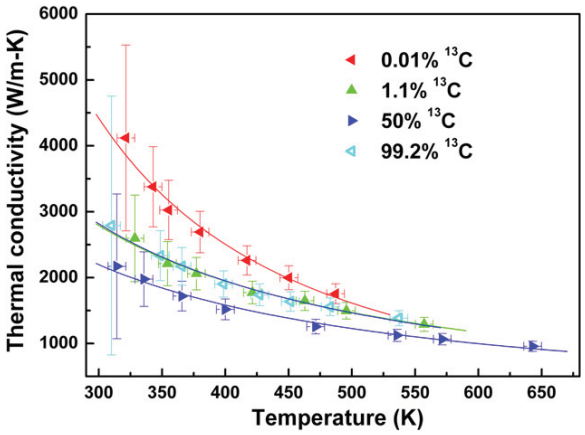

Figure 9. Thermal conductivity of the suspended graphene film with ^{13}C isotope concentrations of 0.01%, 1.1% (natural abundance), 50% and 99.2%, respectively, as a function of the temperature measured using the micro-Raman optothermal technique. Note the strong dependence of thermal conductivity on the isotope concentration. Reproduced with permission from [132]. Copyright 2012 Nature Publishing Group.

an analytical model and MD simulations of the isotope effects in carbon materials, including nanoribbons. The results of the calculations for the thermal conductivity dependence on the isotope composition are in line with the measurements [132]. It was also predicted theoretically that further reduction in thermal conductivity of the isotopically engineered graphene [138] could be achieved if the isotopes were organized in small size clusters rather than being distributed randomly [139]. These findings are in line with those obtained for rectangular GNRs [140].

11. Conclusions

We have reviewed theoretical and experimental results pertinent to 2D phonon transport in graphene. Phonons are the dominant heat carriers in the ungated graphene samples near room temperature. The unique nature of 2D phonons, revealed in very large phonon MFP and peculiarities of the density of states, translates to unusual heat conduction properties of graphene and related materials. We analyzed available computational data for the relative contributions of different phonon polarization branches (LA and TA versus ZA) to heat conduction. Uncertainties associated with various assumptions made in calculation of thermal conductivity have also been discussed. Recent computational studies suggest that the thermal conductivity of graphene depends strongly on the concentration of defects, strain distribution, sample size and geometry. The revealed dependence can account for a portion of the data scatter in reported experimental studies. Investigation of the physics of 2D phonons in graphene can shed light on the thermal energy transfer in low-dimensional systems. The results presented in this review are important for the proposed electronic and optoelectronic applications of graphene, and may lead to new methods of heat removal and thermal management.

Acknowledgments

This work was supported, in part, by the National Science Foundation (NSF) projects US EECS-1128304, EECS-1124733 and EECS-1102074, by the US Office of Naval Research (ONR) through award N00014-10-1-0224, the Semiconductor Research Corporation (SRC) and Defense Advanced Research Project Agency (DARPA) through the FCRP Center on Functional Engineered Nano Architectonics (FENA), and DARPA-DMEA under agreement H94003-10-2-1003. DLN acknowledges financial support through Moldova State Project No 11.817.05.10F. The authors are indebted to Professor Irena Knezevic (UWM) for critical reading of the manuscript and to Drs Natalio Mingo (CEA-Grenoble) and Zlatan Aksamija (UWM) and Professors Xiulin Ruan (Purdue), Aaron P Wemhoff (VU) and Eric Pop (UIUC) for their useful comments on the *arxiv* version of the paper.

Note added in proof. We became aware of a new review focused on MD simulations of the thermal conductivity of graphene [141]. Recent works [142–144] indicate that the excellent phonon transport properties of graphene can be used for applications in thermal interface materials (TIMs).

References

[1] Balandin A A 2009 Better computing through CPU cooling *IEEE Spectr.* **46** 34–9
[2] Pop E 2010 Energy dissipation and transport in nanoscale devices *Nano Res.* **3** 147
[3] Balandin A and Wang K L 1998 Effect of phonon confinement on the thermoelectric figure of merit of quantum wells *J. Appl. Phys.* **84** 6149
[4] Borca-Tasciuc T, Achimov D, Liu W L, Chen G, Ren H-W, Lin C-H and Pei S S 2001 Thermal conductivity of InAs/AlSb superlattices *Microscale Thermophys. Eng.* **5** 225
[5] Li D, Wu Y, Kim P, Shi L, Yang P and Majumdar A 2003 Thermal conductivity of individual silicon nanowires *Appl. Phys. Lett.* **83** 2934
[6] Balandin A A, Pokatilov E P and Nika D L 2007 Phonon engineering in hetero- and nanostructures *J. Nanoelectron. Optoelectron.* **2** 140
[7] Pokatilov E P, Nika D L and Balandin A A 2005 Acoustic-phonon propagation in rectangular semiconductor nanowires with elastically dissimilar barriers *Phys. Rev.* B **72** 113311
[8] Pokatilov E P, Nika D L and Balandin A A 2005 Acoustic phonon engineering in coated cylindrical nanowires *Superlatt. Microstruct.* **38** 168
[9] Liu W and Asheghi M 2006 Thermal conductivity measurements of ultra-thin single crystal silicon layers *J. Heat Transfer* **128** 75
[10] Nika D L, Zincenco N D and Pokatilov E P 2009 Engineering of thermal fluxes in phonon mismatched heterostructures *J. Nanoelectron. Optoelectron.* **4** 180
[11] Lepri S, Livi R and Politi A 2003 Thermal conduction in classical low-dimensional lattices *Phys. Rep.* **377** 1
[12] Basile G, Bernardin C and Olla S 2006 Momentum conversion model with anomalous thermal conductivity in low dimensional system *Phys. Rev. Lett.* **96** 204303
[13] Pokatilov E P, Nika D L and Balandin A A 2003 Phonon spectrum and group velocities in AlN/GaN/AlN and related heterostructures *Superlatt. Microstruct.* **33** 155
[14] Pernot G *et al* 2010 Precise control of thermal conductivity at the nanoscale through individual phonon-scattering barriers *Nature Mater.* **9** 491
[15] Nika D L, Pokatilov E P, Balandin A A, Fomin V M, Rastelli A and Schmidt O G 2011 Reduction of lattice thermal conductivity in one-dimensional quantum-dot superlattices due to phonon filtering *Phys. Rev.* B **84** 165415
[16] Chang C W, Okawa D, Garcia H, Majumdar A and Zettl A 2008 Breakdown of Fourier's law in nanotube thermal conductors *Phys. Rev. Lett.* **101** 075903
[17] Narayan O and Ramaswamy S 2002 Anomalous heat conduction in one dimensional momentum-conserving systems *Phys. Rev. Lett.* **89** 200601
[18] Balandin A A 2011 Thermal properties of graphene and nanostructured carbon materials *Nature Mater.* **10** 569
[19] Cahill D G, Ford W K, Goodson K E, Mahan G D, Majumdar A, Maris H J, Merlin R and Phillpot S R 2003 Nanoscale thermal transport *J. Appl. Phys.* **93** 793
[20] Bhandari C M and Rowe D M 1988 *Thermal Conduction in Semiconductors* (New York: Wiley)
[21] Srivastava G P 1990 *The Physics of Phonons* (Bristol: Taylor and Francis)
[22] Mills A F 1995 *Heat and Mass Transfer* (Chicago, IL: Richard D Irwin) p 62
[23] Ziman J M 2001 *Principles of the Theory of Solids* second edn (New York: Cambridge University Press) p 232
[24] Pierson H O 2010 *Handbook of Carbon, Graphite, Diamonds and Fullerenes: Processing, Properties and Applications* (New Jersey, NJ: Noyes)
[25] Klemens P G 2000 Theory of the a-plane thermal conductivity of graphite *J. Wide Bandgap Mater.* **7** 332
[26] Klemens P G 1958 Thermal conductivity and lattice vibrational modes *Solid State Physics* vol 7, ed F Seitz and D Turnbull (New York: Academic) p 1
[27] Callaway J 1959 Model for lattice thermal conductivity at low temperatures *Phys. Rev.* **113** 1046
[28] Parrott J E and Stuckes A D 1975 *Thermal Conductivity of Solids* (New York: Methuen)
[29] Ziman J M 2001 *Electrons and Phonons: The Theory of Transport Phenomena in Solids* (New York: Oxford University Press)
[30] Balandin A and Wang K L 1998 Significant decrease of the lattice thermal conductivity due to phonon confinement in a free-standing semiconductor quantum well *Phys. Rev.* B **58** 1544
[31] Zou J and Balandin A 2001 Phonon heat conduction in a semiconductor nanowires *J. Appl. Phys.* **89** 2932
[32] Balandin A A 2005 Nanophononics: phonon engineering in nanostructures and nanodevices *J. Nanosci. Nanotechnol.* **5** 1015
[33] Aksamija Z and Knezevic I 2010 Anisotropy and boundary scattering in the lattice thermal conductivity of silicon nanomembranes *Phys. Rev.* B **82** 045319
[34] Soffer S B 1967 Statistical model for the size effect in electrical conduction *J. Appl. Phys.* **38** 1710
[35] Balandin A A, Ghosh S, Bao W, Calizo I, Teweldebrhan D, Miao F and Lau C N 2008 Superior thermal conductivity of single layer graphene *Nano Lett.* **8** 902
[36] Ghosh S, Calizo I, Teweldebrhan D, Pokatilov E P, Nika D L, Balandin A A, Bao W, Miao F and Lau C N 2008 Extremely high thermal conductivity in graphene: prospects for thermal management application in nanoelectronic circuits *Appl. Phys. Lett.* **92** 151911
[37] Ghosh S, Nika D L, Pokatilov E P and Balandin A A 2009 Heat conduction in graphene: experimental study and theoretical interpretation *New J. Phys.* **11** 095012
[38] Ghosh S, Bao W, Nika D L, Subrina S, Pokatilov E P, Lau C N and Balandin A A 2010 Dimensional crossover of thermal transport in few-layer graphene *Nature Mater.* **9** 555

[39] Balandin A A, Ghosh S, Nika D L and Pokatilov E P 2010 Extraordinary thermal conductivity of graphene: possible applications in thermal management *ECS Trans.* **28** 63

[40] Balandin A A, Ghosh S, Nika D L and Pokatilov E P 2010 Thermal conduction in suspended graphene layers *Fullerenes Nanotubes Carbon Nanostruct.* **18** 1

[41] Cai W, Moore A L, Zhu Y, Li X, Chen S, Shi L and Ruoff R S 2010 Thermal transport in suspended and supported monolayer graphene grown by chemical vapor deposition *Nano Lett.* **10** 1645

[42] Jauregui L A *et al* 2010 Thermal transport in graphene nanostructures: experiments and simulations *ECS Trans.* **28** 73

[43] Faugeras C, Faugeras B, Orlita M, Potemski M, Nair R R and Geim A K 2010 Thermal conductivity of graphene in Corbino membrane geometry *ACS Nano* **4** 1889

[44] Lee J U, Yoon D, Kim H, Lee S W and Cheong H 2011 Thermal conductivity of suspended pristine graphene measured by Raman spectroscopy *Phys. Rev.* B **83** 081419

[45] Mak K F, Shan J and Heinz T F 2011 Seeing many-body effects in single and few layer graphene: observation of two-dimensional saddle point excitons *Phys. Rev. Lett.* **106** 046401

[46] Kim K S, Zhao Y, Jang H, Lee S Y, Kim J M, Kim K S, Ahn J, Kim P, Choi J and Hong B H 2009 Large-scale pattern growth of graphene films for stretchable transparent electrodes *Nature* **457** 706

[47] Kravets V G, Grigorenko A N, Nair R R, Blake P, Anissimova S, Novoselov K S and Geim A K 2010 Spectroscopic ellipsometry of graphene and an exciton-shifted van Hove peak in absorption *Phys. Rev.* B **81** 155413

[48] Chen S *et al* 2011 Raman measurement of thermal transport in suspended monolayer graphene of variable sizes in vacuum and gaseous environments *ACS Nano* **5** 321

[49] Seol J H *et al* 2010 Two-dimensional phonon transport in supported graphene *Science* **328** 213

[50] Saito K and Dhar A 2010 Heat conduction in a three dimensional anharmonic crystal *Phys. Rev. Lett.* **104** 040601

[51] Zhong W R, Zhang M P, Ai B Q and Zheng D Q 2011 Chirality and thickness-dependent thermal conductivity of few-layer graphene: a molecular dynamics study *Appl. Phys. Lett.* **98** 113107

[52] Berber S, Kwon Y-K and Tomanek D 2000 Unusually high thermal conductivity in carbon nanotubes *Phys. Rev. Lett.* **84** 4613

[53] Lindsay L, Broido D A and Mingo N 2011 Flexural phonons and thermal transport in multilayer graphene and graphite *Phys. Rev.* B **83** 235428

[54] Singh D, Murthy J Y and Fisher T S 2011 Mechanism of thermal conductivity reduction in few-layer graphene *J. Appl. Phys.* **110** 044317

[55] Jang W, Chen Z, Bao W, Lau C N and Dames C 2010 Thickness-dependent thermal conductivity of encased graphene and ultrathin graphite *Nano Lett.* **10** 3909

[56] Novoselov K S, Geim A K, Morozov S V, Jiang D, Zhang Y, Dubonos S V, Grigorieva I V and Firsov A A 2004 Electric field effect in atomically thin carbon films *Science* **306** 666

[57] Novoselov K S, Geim A K, Morozov S V, Jiang D, Katsnelson M I, Grigorieva I V, Dubonosov S V and Firsov A A 2005 Two-dimensional gas of massless Dirac fermions in graphene 2005 *Nature* **438** 197

[58] Zhang Y B, Tan Y W, Stormer H L and Kim P 2005 Experimental observation of the quantum Hall effect and Berry's phase in graphene *Nature* **438** 201

[59] Evans W J, Hu L and Keblinsky P 2010 Thermal conductivity of graphene ribbons from equilibrium molecular dynamics: effect of ribbon width, edge roughness, and hydrogen termination *Appl. Phys. Lett.* **96** 203112

[60] Munoz E, Lu J and Yakobson B I 2010 Ballistic thermal conductance of graphene ribbons *Nano Lett.* **10** 1652

[61] Savin A V, Kivshar Y S and Hu B 2010 Suppression of thermal conductivity in graphene nanoribbons with rough edges *Phys. Rev.* B **82** 195422

[62] Maultzsch J, Reich S, Thomsen C, Requardt H and Ordejon P 2004 Phonon dispersion in graphite *Phys. Rev. Lett.* **92** 075501

[63] Mohr M, Maultzsch J, Dobardzic E, Reich S, Milosevic I, Damnjanovic M, Bosak A, Krisch M and Thomsen C 2007 Phonon dispersion of graphite by inelastic x-ray scattering *Phys. Rev.* B **76** 035439

[64] Mounet N and Marzari N 2005 First-principles determination of the structural, vibrational and thermodynamic properties of diamond, graphite, and derivatives *Phys. Rev.* B **71** 205214

[65] Wirtz L and Rubio A 2004 The phonon dispersion of graphite revisited *Solid State Commun.* **131** 141

[66] Yan J-A, Ruan W Y and Chou M Y 2008 Phonon dispersions and vibrational properties of monolayer, bilayer, and trilayer graphene: density-functional perturbation theory *Phys. Rev.* B **77** 125401

[67] Falkovsky L A 2008 Symmetry constraints on phonon dispersion in graphene *Phys. Lett.* A **372** 5189

[68] Perebeinos V and Tersoff J 2009 Valence force model for phonons in graphene and carbon nanotubes *Phys. Rev.* B **79** 241409(R)

[69] Lindsay L and Broido D 2010 Optimized Tersoff and Brenner empirical potential parameters for lattice dynamics and phonon thermal transport in carbon nanotubes and graphene *Phys. Rev.* B **81** 205441

[70] Dnbay O and Kresse G 2003 Accurate density functional calculations for the phonon dispersion relation of graphite layer and carbon nanotubes *Phys. Rev.* B **67** 035401

[71] Wang H, Wang Y, Cao X, Feng M and Lan G 2009 Vibrational properties of graphene and graphene layers *J. Raman Spectrosc.* **40** 1791

[72] Mazzamuto F, Saint-Martin J, Valentin A, Chassat C and Dollfus P 2011 Edge shape effect on vibrational modes in graphene nanoribbons: a numerical study *J. Appl. Phys.* **109** 064516

[73] Tan Z W, Wang J-S and Gan C K 2011 First-principles study of heat transport properties of graphene nanoribbons *Nano Lett.* **11** 214

[74] Droth M and Burkard G 2011 Acoustic phonon and spin relaxation in graphene nanoribbons *Phys. Rev.* B **84** 155404

[75] Qian J, Allen M J, Yang Y, Dutta M and Stroscio M A 2009 Quantized long-wavelength optical phonon modes in graphene nanoribbon in the elastic continuum model *Superlatt. Microstruct.* **46** 881

[76] Nika D L, Pokatilov E P, Askerov A S and Balandin A A 2009 Phonon thermal conduction in graphene: role of Umklapp and edge roughness scattering *Phys. Rev.* B **79** 155413

[77] Lui C H, Li Z, Chen Z, Klimov P V, Brus L E and Heinz T F 2011 Imaging stacking order in few-layer graphene *Nano Lett.* **11** 164

[78] Cong C, Yu T, Sato K, Shang J, Saito R, Dresselhaus G F and Dresselhaus M S 2011 Raman characterization of ABA- and ABC-stacked trilayer graphene *ACS Nano* **5** 8760

[79] Calizo I, Balandin A A, Bao W, Miao F and Lau C N 2007 Temperature dependence of the Raman spectra of graphene and graphene multilayers *Nano Lett.* **7** 2645

[80] Graf D, Molitor F, Ensslin K, Stampfer C, Jungen A, Hierold C and Wirtz L 2007 Spatially resolved Raman spectroscopy of single- and few-layer graphene *Nano Lett.* **7** 238

[81] Aksamija Z and Knezevic I 2011 Lattice thermal conductivity of graphene nanoribbons: anisotropy and edge roughness scattering *Appl. Phys. Lett.* **98** 141919

[82] Aizawa T, Sounda R, Otani S, Ishizawa Y and Oshima C 1990 Bond softening in monolayer graphite formed on transition-metal carbide surfaces *Phys. Rev.* B **42** 11469

[83] Pople J A and Musgrave J P 1962 A general valence force field for diamond *Proc. R. Soc.* A **268** 474

[84] Keating P N 1996 Effect of invariance requirements on the elastic strain energy of crystals with application to the diamond structure *Phys. Rev.* **145** 637

[85] Martin R M 1970 Elastic properties of ZnS structure semiconductors *Phys. Rev.* B **1** 4005

[86] Kim P, Shi L, Majumdar A and McEuen P L 2001 Thermal transport measurement of individual multiwalled nanotubes *Phys. Rev. Lett.* **87** 215502

[87] Lippi A and Livi R 2000 Heat conduction in two-dimensional nonlinear lattices *J. Stat. Phys.* **100** 1147

[88] Yang L 2002 Finite heat conductance in a 2D disorder lattice *Phys. Rev. Lett.* **88** 094301

[89] Dhar A 2001 Heat conduction in the disordered harmonic chain revisited *Phys. Rev. Lett.* **86** 5882

[90] Casher A and Lebowitz J L 1971 Heat flow in regular and disordered harmonic chains *J. Math. Phys.* **12** 1701

[91] Ecsedy D J and Klemens P G 1977 Thermal resistivity of dielectric crystals due to 4-phonon processes and optical modes *Phys. Rev.* B **15** 5957

[92] Mingo N and Broido D 2005 Length dependence of carbon nanotube thermal conductivity and the problem of long waves *Nano Lett.* **5** 1221

[93] Lindsay L, Broido D A and Mingo N 2010 Diameter dependence of carbon nanotube thermal conductivity and extension to the graphene limit *Phys. Rev.* B **82** 161402

[94] Klemens P G 2001 Theory of thermal conduction in the ceramic films *Int. J. Thermophys.* **22** 265

[95] Nika D L, Ghosh S, Pokatilov E P and Balandin A A 2009 Lattice thermal conductivity of graphene flakes: comparison with bulk graphite *Appl. Phys. Lett.* **94** 203103

[96] Kelly B T 1981 *Physics of Graphite* (London: Applied Science)

[97] Kong B D, Paul S, Nardelli M B and Kim K W 2009 First-principles analysis of lattice thermal conductivity in monolayer and bilayer graphene *Phys. Rev.* B **80** 033406

[98] Nika D L, Pokatilov E P and Balandin A A 2011 Theoretical description of thermal transport in graphene: the issues of phonon cut-off frequencies and polarization branches *Phys. Status Solidi* b **248** 2609

[99] Jiang J-W, Wang J-S and Li B 2009 Thermal conductance of graphite and dimerite *Phys. Rev.* B **79** 205418

[100] Huang Z, Fisher T S and Murthy J Y 2010 Simulation of phonon transmission through graphene and graphene nanoribbons with a Green's function method *J. Appl. Phys.* **108** 094319

[101] Hu J, Ruan X and Chen Y P 2009 Thermal conductivity and thermal rectification in graphene nanoribbons: a molecular dynamic study *Nano Lett.* **9** 2730

[102] Guo Z, Zhang D and Gong X-G 2009 Thermal conductivity of graphene nanoribbons *Appl. Phys. Lett.* **95** 163103

[103] Zhai X and Jin G 2011 Stretching-enhanced ballistic thermal conductance in graphene nanoribbons *Europhys. Lett.* **96** 16002

[104] Jinag J-W, Wang B-S and Wang J-S 2011 First principle study of the thermal conductance in graphene nanoribbon with vacancy and substitutional silicon defects *Appl. Phys. Lett.* **98** 113114

[105] Ouyang T, Chen Y P, Yang K K and Zhong J X 2009 Thermal transport of isotopic-superlattice graphene nanoribbons with zigzag edge *Europhys. Lett.* **88** 28002

[106] Wang Z and Mingo N 2011 Absence of Casimir regime in two-dimensional nanoribbon phonon conduction *Appl. Phys. Lett.* **99** 101903

[107] Hu J, Wang Y, Vallabhaneni A, Ruan X and Chen Y 2011 Nonlinear thermal transport and negative differential thermal conductance in graphene nanoribbons *Appl. Phys. Lett.* **99** 113101

[108] Xie Z-X, Chen K-Q and Duan W 2011 Thermal transport by phonons in zigzag graphene nanoribbons with structural defects *J. Phys.: Condens. Matter* **23** 315302

[109] Murali R, Yang Y, Brenner K, Beck T and Meindl J D 2009 Breakdown current density of graphene nanoribbons *Appl. Phys. Lett.* **94** 243114

[110] Liao A D, Wu J Z, Wang X, Tahy K, Jena D, Dai H and Pop E 2011 Thermally limited current carrying ability of graphene nanoribbons *Phys. Rev. Lett.* **106** 256801

[111] Qiu B and Ruan X 2011 Molecular dynamics simulations of thermal conductivity and spectral phonon relaxation time in suspended and supported graphene, arXiv:111.4613v1

[112] Zhang H, Lee G and Cho K 2011 Thermal transport in graphene and effects of vacancies *Phys. Rev.* B **84** 115460

[113] Lindsay L, Broido D A and Mingo N 2010 Flexural phonons and thermal transport in graphene *Phys. Rev.* B **82** 115427

[114] Wei Z, Ni Z, Bi K, Chen M and Chen Y 2011 In-plane lattice thermal conductivities of multilayer graphene films *Carbon* **49** 2653

[115] Ong Z-Y and Pop E 2011 Effect of substrate modes on thermal transport in supported graphene *Phys. Rev.* B **84** 075471

[116] Qiu B and Ruan X 2011 Mechanism of thermal conductivity reduction from suspended to supported graphene: a quantitative spectral analysis of phonon scattering *Proc. ASME 2011 Mechanical Engineering Congr. & Exposition ASME Paper IMECE2011 62963*

[117] Wei N, Xu L, Wang H-Q and Zheng J-C 2011 Strain engineering of thermal conductivity in graphene sheets and nanoribbons: a demonstration of magic flexibility *Nanotechnology* **22** 105705

[118] Hao F, Fang D and Xu Z 2011 Mechanical and thermal transport properties of graphene with defects *Appl. Phys. Lett.* **99** 041901

[119] Klemens P G and Pedraza D F 1994 Thermal conductivity of graphite in basal plane *Carbon* **32** 735

[120] Singh D, Murthy J Y and Fisher T S 2011 On the accuracy of classical and long wavelength approximations for phonon transport in graphene *J. Appl. Phys.* **110** 113510

[121] Broido D A, Ward A and Mingo N 2005 Lattice thermal conductivity of silicon from empirical interatomic potentials *Phys. Rev.* B **72** 014308

[122] Cowley E R 1988 Lattice dynamics of silicon with empirical many-body potentials *Phys. Rev. Lett.* **60** 2379

[123] Sevincli H, Li W, Mingo N, Cuniberti G and Roche S 2011 Effects of domains in phonon conduction through hybrid boron nitride and graphene sheets *Phys. Rev.* B **84** 205444

[124] Esfarjani K, Chen G and Stokes H T 2011 Heat transport in silicon from first-principles calculations *Phys. Rev.* B **84** 085204

[125] Ho C Y, Powell R W and Liley P E 1974 Thermal conductivity of the elements: a comprehensive review *J. Phys. Chem. Ref. Data* **3** 1

[126] Woodcraft A L, Barucci M, Hastings P R, Lolli L, Martelli V, Risegari L and Ventura G 2009 Thermal conductivity measurements of pitch-bonded at millikelvin temperatures: finding a replacement for AGOT graphite *Cryogenics* **49** 159

[127] Wei L, Kuo P K, Thomas R L, Anthony T R and Banholzer W F 1993 Thermal diffusivity of isotopically modified single crystal diamond *Phys. Rev. Lett.* **70** 3764

[128] Anthony T R, Banholzer W F, Fleischer J F, Wei L, Kuo P K, Thomas R L and Pryor R W 1990 Thermal diffusivity of isotopically enriched ^{12}C diamond *Phys. Rev.* B **42** 1104

[129] Bray J W and Anthony T R 1991 On the thermal conductivity of diamond under changes of its isotopic character *Z. Phys.* B **84** 51

[130] Ager J W and Haller E E 2006 Isotopically engineered semiconductors: from bulk to nanostructures *Phys. Status Solidi* a **203** 3550
[131] Ramirez A P, Kortan A R, Rosseinsky M J, Duclos S J, Mujsce A M, Haddon R C, Murphy D W, Makhija A V, Zahurak S M and Lyons K B 1992 Isotope effects in superconducting Rb_3C_{60} *Phys. Rev. Lett.* **68** 1058
[132] Chen S, Wu Q, Mishra C, Kang J, Zhang H, Cho K, Cai W, Balandin A A and Ruoff R S 2012 Thermal conductivity of isotopically modified graphene *Nature Mater.* **11** 203
[133] Li X, Magnuson C W, Venugopal A, Tromp R M, Hannon J B, Vogel E M, Colombo L and Ruoff R S 2011 Large area graphene single crystals grown by low pressure chemical vapor deposition of methane on copper *J. Am. Chem. Soc.* **133** 2816
[134] Li X S, Cai W W, Colombo L and Ruoff R S 2009 Evolution of graphene growth on Ni and Cu by carbon isotope labeling *Nano Lett.* **9** 4268
[135] Jiang J W, Lan J H, Wang J S and Li B W 2010 Isotopic effects on the thermal conductivity of graphene nanoribbons: localization mechanism *J. Appl. Phys.* **107** 054314
[136] Zhang H, Lee G, Fonseca A F, Borders T L and Cho K 2010 Isotope effect on the thermal conductivity of graphene *J. Nanomater.* **2010** 537657
[137] Balasubramanian G, Puri I K, Bohm M C and Leroy F 2011 Thermal conductivity reduction through isotope substitution in nanomaterials: predictions from an analytical classical model and nonequilibrium molecular dynamics simulations *Nanoscale* **3** 3714
[138] Savic I, Mingo N and Stewart D A 2008 Phonon transport in isotope-disordered carbon and boron-nitride nanotubes: is localization observable? *Phys. Rev. Lett.* **101** 165502
[139] Mingo N, Esfarjani K, Broido D A and Stewart D A 2010 Cluster scattering effects on phonon conduction in graphene *Phys. Rev.* B **81** 045408
[140] Hu J, Schiffli S, Vallabhaneni A, Ruan X and Chen Y P 2010 Tuning the thermal conductivity of graphene nanoribbons by edge passivation and isotope engineering: a molecular dynamics study *Appl. Phys. Lett.* **97** 133107
[141] Wemhoff A P 2012 A review of theoretical techniques for graphene and graphene nanoribbon thermal conductivity prediction *Int. J. Transport Phenom.* at press
[142] Shahil K M F and Balandin A A 2012 Graphene-multilayer graphene nanocomposites as highly efficient thermal interface materials *Nano Lett.* **12** 861
[143] Goyal V and Balandin A A 2012 Thermal properties of the hybrid graphene–metal nano-micro-composites: applications in thermal interface materials *Appl. Phys. Lett.* **100** 073113
[144] Shahil K M F and Balandin A A 2012 Thermal properties of graphene and multilayer graphene: applications in thermal interface materials *Solid State Commun.* at press